MINISTÉRIO DA EDUCAÇÃO
UNIVERSIDADE FEDERAL DO RIO GRANDE DO SUL
PROGRAMA DE PÓS-GRADUAÇÃO EM ENGENHARIA MECÂNICA

AN INTEGRAL EQUATION FORMULATION FOR 2D STEADY-STATE ADVECTION-DIFFUSION-REACTION PROBLEMS WITH VARIABLE COEFFICIENTS

por

Luiz Fernando Bez

Dissertação para obtenção do Título de
Mestre em Engenharia

Porto Alegre, Março de 2020

AN INTEGRAL EQUATION FORMULATION FOR 2D STEADY-STATE ADVECTION-DIFFUSION-REACTION PROBLEMS WITH VARIABLE COEFFICIENTS

por

Luiz Fernando Bez
Engenheiro

Dissertação submetida ao Corpo Docente do Programa de Pós-Graduação em Engenharia Mecânica, PROMEC, da Escola de Engenharia da Universidade Federal do Rio Grande do Sul, como parte dos requisitos necessários para a obtenção do Título de

Mestre em Engenharia

Área de Concentração: Fenômenos de Transporte

Orientador: Prof. Dr. Marco Tullio Menna Barreto de Vilhena
Co-Orientador: Prof. Dr. Rogério Marczak

Aprovada por:

Ricardo Carvalho de Barros ..... IPRJ/UERJ

Rejane De Césaro Oliveski ..... UNISINOS

Adriane Prisco Petry ..... PROMEC/UFRGS

Prof. Dr. Fernando Marcelo Pereira
Coordenador do PROMEC

Porto Alegre, 6 de Março de 2020

RESUMO

Este trabalho apresenta uma formulação de equação integral de contorno e domínio para problemas de advecção-difusão-reação com coeficientes variáveis e termo fonte. A formulação usa uma versão da solução fundamental que evita *overflow* numérico dos termos exponenciais e *underflow* dos termos em função de Bessel, para qualquer número de Péclet e qualquer tamanho de domínio. Os coeficientes usados na solução fundamental são os coeficientes locais da equação diferencial, afim de minimizar a contribuição do domínio no problema. A formulação é aplicada sem modificações para problemas puramente difusivos ou de difusão-reação. A equação integral é discretizada usando o método dos elementos de contorno, com elementos de contorno contínuos e células de domínio descontínuas. O método é validado com cinco problemas de *benchmark* que possuem soluções analíticas, apresentando um erro NRMSD abaixo de 1% para malhas com 1348 graus de liberdade, em todos os casos. A metodologia é usada para o estudo de dois problemas práticos. O primeiro é o problema de Graetz-Nusselt adimensional para $Pe = \{0, 1, 5, 10\}$. O segundo é um problema de pluma de dispersão de poluentes para uma fonte pontual em escoamentos de camada limite atmosférica neutramente estratificada.

Palavras-chave: Equação integral; Método dos elementos de contorno; Transporte escalar; Fonte pontual.

ABSTRACT

This work presents a boundary-domain integral equation formulation for advection-diffusion-reaction problems with variable coefficients and source term. The formulation uses a version of the fundamental solution that avoids numerical overflow of the exponential term and underflow of the Bessel term, for any Péclet number and domain size. Furthermore, the coefficients used in the fundamental solution are the local coefficients of the differential equation, in order to minimize the domain contribution for the problem. The formulation is applied as-is for purely diffusive or diffusion-reaction problems. The integral equation is discretized using the boundary element method with continuous boundary elements and discontinuous domain cells. The scheme is validated against five benchmark problems with analytical solutions, presenting a NRMSD error under 1% for meshes with 1348 degrees of freedom, in all cases. The methodology is used to study two practical problems. The first is the dimensionless Graetz-Nusselt problem for $Pe = \{0, 1, 5, 10\}$. The second is the pollutant dispersion plume for a point source in neutrally stratified atmospheric boundary layer flows.

Keywords: Integral equation; Boundary element method; Scalar transport; Point source.

AGRADECIMENTOS

Primeiramente agradeço aos Professores Marco e Rogério, por todos os conselhos e pela confiança depositada em mim durante a orientação desse trabalho.

Agradeço aos membros da banca de avaliação, Professores Ricardo, Rejane e Adriane, pelas contribuições à este trabalho.

Agradeço a todos os companheiros do GMAp, nossas incontáveis discussões, técnicas ou não, contribuíram para enriquecer este trabalho e para tornar os meses de trabalho mais agradáveis.

Agradeço ao Conselho Nacional de Desenvolvimento Científico e Tecnológico (CNPq) pelo suporte financeiro para a elaboração deste trabalho.

Por fim, agradeço a minha família, pelo incentivo ao estudo que sempre me deram, pelo suporte e pelo carinho.

TABLE OF CONTENTS

LIST OF FIGURES

LIST OF TABLES

LIST OF ACRONYMS AND ABBREVIATIONS

ASME	American Society of Mechanical Engineers
BEM	Boundary Element Method
BDIDE	Boundary-Domain Integro-Differential Equation
BDIE	Boundary-Domain Integral Equation
CPV	Cauchy Principal Value
DR	Dual Reciprocity
FEM	Finite Element Method
FVM	Finite Volume Method
RANS	Reynolds Averaged Navier-Stokes
RIBEM	Radial Integration Boundary Element Method
WRM	Weighted Residual Method

LIST OF SYMBOLS

Latin Symbols

a_j	Linear coefficient of ψ_j
$\boldsymbol{b}^b$	Vector corresponding to the source effect for collocation points at the boundary
$\boldsymbol{b}^d$	Vector corresponding to the source effect for collocation points in the domain
$\boldsymbol{B}^b$	Coefficient matrix corresponding to the domain values of ϕ for collocation points at the boundary
$\boldsymbol{B}^d$	Coefficient matrix corresponding to the domain values of ϕ for collocation points in the domain
b_j	Constant coefficient of ψ_j
C	Friction velocity divided by the Von Kárman constant, m/s
c_ξ	$\mathbb{R}^2 \to [0,1]$, Free coefficient that varies according to the location of the fundamental solution's source point
c_b	$b = 1, 2, 3$, Auxiliary constants for the variable-velocity benchmark
d	$d : \Omega \to \mathbb{R}_{>0}$, Diffusivity field, m^2/s
d_ξ	$d(\xi)$, Diffusivity at the point ξ, m^2/s
D_j	Relative deviation form mesh j in relation to mesh $j-1$
$\mathrm{d}A$	Two-dimensional differential, m^2
$\mathrm{d}l$	One-dimensional differential, m
E_1	$E_1 \in \mathbb{R}$, NRMSD estimator for the boundary values of ϕ
E_2	$E_2 \in \mathbb{R}$, NRMSD estimator for the boundary values of q_n
E_3	$E_3 \in \mathbb{R}$, NRMSD estimator for the domain values of ϕ
f	$f : [-1,1] \to \mathbb{R}$, Generic Kernel for one-dimensional integrals
f_i^j	Value at point i, referring to the j-th mesh, used for discretization studies
$\boldsymbol{G}^b$	Coefficient matrix corresponding to the boundary values of q_n for collocation points at the boundary
$\boldsymbol{G}^d$	Coefficient matrix corresponding to the boundary values of q_n for collocation points in the domain

$\boldsymbol{H}^b$	Coefficient matrix corresponding to the boundary values of ϕ for collocation points at the boundary
$\boldsymbol{H}^d$	Coefficient matrix corresponding to the boundary values of ϕ for collocation points in the domain
h	Increment used in the definition of a derivative
h_c	Cell edge size
h_e	Boundary element length
I_j	j-th reference integral used in the study of quadrature order
k	$k : \Omega \to \mathbb{R}$, Linear source term, 1/s
k_ξ	$k(\xi)$, Linear source term at the point ξ, 1/s
K_ν	$\mathrm{K}_\nu : \mathbb{R}_{>0} \to \mathbb{R}_{>0}$, Modified Bessel function of the second kind and order ν
K^*_ν	$\mathrm{K}^*_\nu : \mathbb{R}_{>0} \to \mathbb{R}_{>0}$, Scaled modified Bessel function of the second kind and order ν, given by $\exp(x)\mathrm{K}_\nu(x)$
L	Generic linear differential operator
l_e	Length of a generic boundary element, m
$\boldsymbol{n}$	Unitary vector outward normal do the boundary $\partial\Omega$
n_f	Number of sample values used for the mesh quality study
n_g	Number of quadrature points
n_j	Number of boundary nodes
n_k	Number of point sources in the domain
n_l	Number of internal nodes
$\mathcal{O}$	Order of magnitude
p_i	$i \in 1, 2, 3, 4$, Auxiliary parameters for the definition of Telles cubic coordinate transformation
Pe	Péclet number
q^*	$q^* : \partial\Omega \to \mathbb{R}$, Derivative of ϕ^* in the direction outward normal to the boundary $\partial\Omega$
q_n	$q_n : \partial\Omega \to \mathbb{R}$, Derivative of ϕ in the direction outward normal to the boundary $\partial\Omega$
$\bar{q_n}$	$\bar{q_n} \in \mathbb{R}$, Reference value of q_n, used in error estimators
q_{nj}	q_n at node j

R	Residual of the application of a differential operator to a given approximate solution
$\boldsymbol{r}$	$\boldsymbol{r} \in \mathbb{R}^2$, Vector denoting the distance to the source point, m
r	$r \in \mathbb{R}_{\geq 0}$, Absolute distance to the source point, m
r_n	$r \in \mathbb{R}$, Distance to the source point along the n direction
r_t	Aggressiveness factor for Telles cubic coordinate transformation
$\mathbb{R}$	Set of real numbers
$\mathbb{R}^2$	$\mathbb{R} \times \mathbb{R}$, Set of pairs of real numbers
$\mathbb{R}_{>0}$	Set of strictly positive real numbers
$\mathbb{R}_{\geq 0}$	Set of real numbers that are greater than or equal to zero
S	$S : \Omega \to \mathbb{R}$, Independent source term, 1/s
S_f	$S_f : \Omega \to \mathbb{R}$, Limited part of the independent source term, 1/s
s_k	Strength of the k-th domain point source, 1/s
t_i	Coefficient from Telles transformation that multiplies ζ_i
T	Temperature field for the Graetz-Nusselt problem, K
T_{in}	Inlet temperature for the Graetz-Nusselt problem, K
T_{wall}	Wall temperature for the Graetz-Nusselt problem, K
u	Generic interpolated variable
u_j	Generic interpolated variable, evaluated at node j
$\boldsymbol{v}$	$\boldsymbol{v} : \Omega \to \mathbb{R}^2$, Velocity field, m/s
$\boldsymbol{v}_\xi$	$\boldsymbol{v}(\xi)$, Velocity vector at the point ξ, m/s
v	$v : \Omega \to \mathbb{R}_{\geq 0}$, Absolute velocity, given by $\sqrt{\boldsymbol{v} \cdot \boldsymbol{v}}$, m/s
v_ξ	$v(\xi)$, Absolute velocity at the point ξ, m/s
v_n	$v_n : \partial\Omega \to \mathbb{R}$, Velocity normal to the boundary, given by $\boldsymbol{v} \cdot \boldsymbol{n}$, m/s
$\boldsymbol{x}_k$	$\boldsymbol{x}_k \in \Omega$, The location of the k-th domain point source
x_g	$x_g \in [-1, 1]$, Gauss-Legendre quadrature points
x_t	$x_t \in [-1, 1]$, Gauss-Legendre quadrature points transformed by Telles technique
y_0	Roughness length, m

Greek Symbols

α	$\alpha \in (0, 1)$, Discontinuity parameter for elements and cells
γ	Angle between the velocity and the distance vector to the source point

δ_ξ	Dirac's delta distribution dislocated to the point ξ
δ_{ij}	Kronecker delta
ζ	Normalized coordinate
η	Normalized coordinate
θ	$\theta \in [0, 2\pi]$, Internal angle of a boundary point
λ	Dimensionless velocity distribution
μ	Auxiliary variable used in the fundamental solution
ν	Order of the modified Bessel function of the second kind
$\boldsymbol{\xi}$	Source point
φ	$\varphi : [-1, 1] \to [-1, 1]$, Telles cubic coordinate mapping
ϕ	$\phi : \Omega \to \mathbb{R}$ Scalar property to be transported
$\bar{\phi}$	$\bar{\phi} \in \mathbb{R}$, Reference value of ϕ
ϕ^*	$\phi^* : \mathbb{R}^2 \to \mathbb{R}$, Weighting function and fundamental solution
ϕ^*_ξ	$\phi^*_\xi : \mathbb{R}^2 \to \mathbb{R}$, Fundamental solution corresponding to a source placed at the point $\xi \in \overline{\Omega}$
ϕ_j	ϕ at node j
ψ_j	Compact support 1D basis function corresponding to the j-th node
Ψ_l	Compact support 2D basis function corresponding to the j-th node
ω_g	Gauss-Legendre quadrature weights
ω_t	Quadrature weights used with Telles transformation
Ω	$\Omega \subset \mathbb{R}^2$, Two-dimensional domain
$\overline{\Omega}$	Closure of Ω
$\partial\Omega$	The domain's boundary, $\overline{\Omega} \setminus \Omega$
$\partial\Omega_D$	Part of the domain's boundary with Dirichlet boundary conditions
$\partial\Omega_N$	Part of the domain's boundary with Neumann boundary conditions

1 INTRODUCTION

The advection-diffusion-reaction equation models critical phenomena, such as heat transfer and pollutant transport. For example, knowing the response of a pollutant source may be vital not only to control the damage of an accidental event but also to project the site of an industrial complex in order to minimize such an event. Also, many industrial applications have to deal with toxic residues in the work environment, and the correct management of such substances represents an important health issue.Therefore, adequately solving that equation may be vital in many engineering projects.

One option is to solve the advective-diffusive-reactive model analytically. However, the analytical methods can be applied to problems with regular domains but not for realistic ones, with complex topography terrain, for example. One alternative is to employ analytical solutions in order to analyze a simplified version of the problem. That approach, however, is only practical for particular circumstances and results in a loss in solution quality when applied to realistic situations [Cunha et al., 2016].

We then choose to use a numerical solution for the aforementioned differential problem - for instance, one of the traditional numerical domain methods, such as the finite volume method (FVM) or the finite element method (FEM). However, problems with a high velocity field and high gradients (such as those from point sources) usually require fine meshing, in turn demanding significant computational time for the numerical simulations [Sharma, 2017].

Another option would be to use the so-called boundary methods, such as the boundary element method (BEM). This particular method is based on an integral equation formulation, and it uses a fundamental solution to rewrite the problem, at least in part, as a boundary problem. Ikeuchi and Onishi, 1983, showed that the BEM could be used as an alternative to domain methods in transport problems, for it decreases the problem size while maintaining solution quality. Also, in cases when the velocity-to-diffusivity ratio becomes too large, the BEM has an additional advantage. The upwind effect of the velocity field is accounted for in the fundamental solution, allowing the mesh used to be coarser and the solution numerically more efficient and stable even for very high local Péclet numbers [Qiu et al., 1998].

The boundary element method has, however, its drawbacks. One of them is an

increase in mathematical complexity, compared to other methods. The functions involved are not as simple, it has singular kernels to be integrated, and the overall structure of the algorithms tends to be more complex as well. The method also generates a matrix system that is asymmetrical and full, resulting in $\mathcal{O}(N^2)$ complexity. As a result, this method is not as popular as the domain ones, especially in transport phenomena [Cheng and Cheng, 2005; Ramachandran, 1998].

Scalar transport problems began to be dealt with by the BEM at the beginning of the '80s [Ikeuchi and Onishi, 1983]. Since then, much has been done in order to broaden the scope of the BEM formulations and solve some of the numerical issues that arise. Modern integral formulations, such as those presented by Ravnik and Škerget, 2013, and Ravnik and Škerget, 2014, use gradient-free versions of boundary-domain integral equations (BDIE) for steady-state and transient problems. These authors present the gradient-free BDIE for advective-diffusive equations with source, and they solve it using both single-domain, and sub-domain BEM. In this work we will expand the formulation proposed by Ravnik and Škerget, 2013, by considering linear reaction terms that also may vary in the domain. In order to treat the domain effects we chose to interpolate them using cells. This may not be the most modern approach, but it is the most direct.

1.1 Objectives

The primary objective of this work is to derive and implement a boundary element scheme to solve an integral equation formulation for 2D steady-state advection-diffusion-reaction problems with variable source and coefficients.

The secondary objectives are as follows:

- Validate the numerical scheme developed against analytical solutions.
- Use the same scheme to solve degenerated forms of the differential equation, such as pure diffusion problems.
- Solve transport problems with point sources and velocity profiles that are compatible with atmospheric flows.

1.2 Dissertation Outline

This work is organized into six additional chapters. Chapter 2 presents a bibliographic review of academic studies. It begins with a brief review of the early origins of the integral equation and boundary element methods, following with a more extensive review of the use of the boundary element method to solve the passive scalar transport problem. Also, the chapter presents a highlight on some of the numerical techniques used to deal with the variable coefficient equation.

Chapter 3 contains the integral formulation used in this work. It begins with the presentation of the differential problem, with all of its suppositions. It follows with the development of the weighted residuals statement, the presentation of the fundamental solution and the inverse problem. A gradient-free version of the integral equation is derived, with the analytical treatment of point sources.

Chapter 4 presents the numerical implementation of the scheme. It begins with the discretization of the boundary and domain, and the assembly of the matrix system. We discuss in length the numerical techniques used to evaluate each component of the matrices, showing their qualitative behavior and the numerical convergence of the chosen integration technique.

Chapter 5 contains benchmarks assessing the performance of the numerical scheme against problems with analytical solutions. The 5 cases were chosen in such a way as to utilize the terms present on the integral equation in at least one problem.

Chapter 6 contains two applications of the method on real problems. The first is the Graetz-Nusselt problem, dealing with heat transfer in a rectangular section for fully developed laminar flow. The second is the pollutant plume formation in neutrally stratified atmospheric boundary layer type flows.

Chapter 7 presents the conclusions of this dissertation. It also contains proposed ways to further the work.

2 LITERATURE REVIEW

In this chapter, we will start by briefly reviewing the origins of the boundary element method in general. We will then follow it with a more detailed review of the application of the method in linear scalar transport problems.

2.1 Origins of the Boundary Element Method

The boundary element method at its core involves the formulation of the problem in terms of its boundary, using a fundamental solution to produce boundary-only integral equations. These integral equations predate the computer age, and, arguably, the origins of these methods can be traced to the beginning of the 20th century [Massonnet and Morelle, 1987]. For instance, Fredholm, 1906, and Lauricella, 1907, produced systems of integral equations that could be numerically implemented with BEM, if computers existed at the time.

In the early 1960s, when electronic computers started to become more widely available to researchers, numerical methods started to become prominent as a way to solve partial differential equations. At the beginning of the decade, for example, Friedman and Shaw, 1962, solved the scalar wave equation via the discretization of a boundary integral form of the problem and Ponter and Jawson, 1963, employed Green's identity to numerically solve bars subjected to torsion.

Despite many works being published using integral equations to solve boundary value problems, the method did not become an integrated movement until the works of Rizzo's article *An integral equation approach to boundary value problems of classical elastostatics* [Rizzo, 1967]. In this paper, a numerical procedure was developed for solving elastostatics problems via the Somigliana's identity.

In 1975 Thomas Allen Cruse and Frank Joseph Rizzo organized the first boundary integral equation method meeting with the support of the American Society of Mechanical Engineers (ASME). The next meeting on this subject was held in 1977. In the same conference, Carlos Alberto Brebbia gave a keynote address on the numerical solution of boundary integral equations using boundary elements.

In the decade of 1970, Brebbia and his research group, notably with Watson and Lachat, worked on improving the versatility of integral equation methods. Lachat finished

his dissertation in 1975 and his paper with Watson. Lachat and Watson, 1976, was considered to be the first to incorporate finite element technologies and techniques on the integral equation framework [Cheng and Cheng, 2005].

In the same decade, following the development of finite elements, it was shown that the weighted residuals techniques could be used to derive the boundary integral equations [Brebbia and Dominguez, 1992, 1977; Brebbia, 1978]. In 1978 Brebbia organized the first international conference on the Boundary Element Method, and published the first textbook on the subject [Cheng and Cheng, 2005].

A more detailed review of the origins of the method can be found in Cheng and Cheng, 2005, and a review on the subsequent developments of the method can be found in Brebbia, 2017.

2.2 Applications on Linear Scalar Transport

Advection-diffusion problems started to be handled by the BEM at the beginning of the 1980s. Ikeuchi and Onishi, 1983, showed convergence and stability for 2D and 3D steady-state problems, also showing that a constant-coefficient problem could be solved using either the Laplace fundamental solution - treating the advective terms analogously to a source - or using the Advection-diffusion fundamental solution, without any domain terms. Brebbia and Skerget, 1984, extended the solution to transient problems, using domain cells to solve the transient part of the problem. Tanaka et al., 1986, 1987, solved the transport problem with variable velocity profiles and compared the solutions to that of FEM schemes. It showed that the stability of the BEM did not depend on the Péclet number, while that of the FEM did. In most transport problems, we have a velocity profile that varies in space, which means that we would need a BEM scheme that has domain dependence. By the end of the decade, we start to see efforts to produced boundary-only procedures, rewriting the domain terms in an approximate form that would involve only boundary integration. Aral and Tang, 1989, does such an effort using secondary reduction in transient 2D problems. It also incorporates first order chemical reaction.

From the '90s onwards, we see an increasing number of papers published on the subject. The rest of this review will be separated by themes rather than by dates. We will begin reviewing the work done on integration, stability, and transient problems using a constant-coefficient equation, and we will follow it with the different numerical techniques

used to deal with increasingly complex forms of the equation.

The kernels arising from the use of the advective-diffusive fundamental solution are, in general, hard to integrate, and their behavior varies with the Péclet number of the problem. Chan and Chandra, 1991, studied the handling of corners in advective-diffusive problems. Qiu et al., 1998, showed the importance of accurate integration, especially for problems with high Péclet numbers, and studied the asymptotic behavior of the fundamental solution and the different kernels involved on the boundary integrals. Singh and Tanaka, 2000, studied analytical integration in BEM for the Helmholtz and the Advection-diffusion equations. Sedaghatjoo and Adibi, 2012, studied the calculation of domain integrals arising in problems with variable coefficients.

High Péclet numbers imply a high directionality to the fundamental solution. A few authors tried to exploit this behavior in order to have more efficient integration by ignoring the terms which would be negligible given the direction of the advective field. Several studies proposed algorithms to selectively integrate elements taking into account this behavior, noticeably Qiu et al., 1998; Grigoriev and Dargush, 2005a,c,b. Dargush and Grigoriev, 2008, expanded this study for domain effects as well. In addition to the directionality, Grigoriev and Dargush, 2004a,b, studied high order boundary elements in that context.

At the beginning of the '90s Li and Evans, 1991, solved advective-diffusive problems with constant coefficients but non-linear boundary conditions. Later on that decade, Li, 1993, explored a similar problem, using exponential transformation and different fundamental solutions.

The constant-coefficient equation was used to model problems of design sensitivity in steady-state cases [Chandra and Chan, 1992], modeling electromagnetism [Enokizono and Nagata, 1992], response to moving sources [Lim et al., 1994], and phase change with moving front and quasi-static modeling [Young et al., 1992; Cholewa et al., 2004]. Driessen and Dohner, 2001, bypassed the changing coefficients problem by coupling FEM on a region with changing velocity with BEM for an unbounded domain where the velocity variations were negligible. Finally, Cunha et al., 2016, used a transient fundamental solution to solve constant coefficient transient problems with no domain effects.

Problems with variable velocity fields were present on publications ever since the BEM started to be applied in advection-diffusion problems. Wrobel and DeFigueiredo,

1991a,b, showed integral formulations for problems with variable velocity fields, both in the form of boundary-domain integral equations (BDIE's) and boundary-domain integro-differential equations (BDIDE's). The difference between the two is that the former is integrated by parts in such a way as to only have primal variable unknowns on the domain, while the latter may also contain dual variables as unknowns on the domain. Ravnik and Škerget, 2013, presented a gradient-free BDIE formulation for an advection-diffusion equation with diffusivity and velocity variable on the domain. Ravnik and Škerget, 2014, expanded that formulation for transient problems with a source term.

Advection-diffusion problems in anisotropic media using BEM gained attention in recent years. Carrer et al., 2017, studied 2D transient problems in anisotropic media using a formulation with the Laplace fundamental solution, one that was already well used for diffusion in anisotropic media. That implied that the advective terms were fully treated as sources. The domain terms were computed with integration in linear triangular cells. Azis et al., 2018, presented a formulation for constant-coefficient problems using the anisotropic advection-diffusion fundamental solution. Azis, 2019, solves the anisotropic equation with variable coefficients using a variable transformation.

One of the characteristics that make the BEM an attractive choice is the reduction in dimension, *i.e.*, only the boundary needs to be discretized. However, in more general problems, where there are transient effects present, and where any of the coefficients of the equation change in space, the need for domain discretization and domain unknowns arises. There are many different ways to deal with these domain effects, and next, we will highlight some of these efforts, notably cell discretization, dual reciprocity (DR), radial integration, and domain decomposition.

2.2.1 Cell Interpolation used in Advection-Diffusion Problems

When domain integrals arise in an integral formulation, perhaps the most straightforward way to approach them is to interpolate the unknown functions using compact support polynomials defined on a mesh formed by cells. These cells do not have the same requirements that, for instance, a finite element mesh would have. They are used only to integrate the domain effects, which are equivalent to a variable source on the formulation. In general, the cells can be bigger in relation to the boundary elements, but that varies in a case-by-case scenario.

Ikeuchi and Onishi, 1983, already showed that the advective terms could be fully modeled using domain cells (using the Laplace fundamental solution). Brebbia and Skerget, 1984, used the advection-diffusion equation and modeled its transient part using cell integration.

Wrobel and DeFigueiredo, 1991a, presented a gradient-free formulation for variable-velocity problems using cell interpolation. The paper shows that, in cases where the Péclet number is high or the domain effects are complex, the cell interpolation is more stable than the dual reciprocity. Still in the nineties, Gupta et al., 1994, explored the steady-state problem with variable velocity using cells, while Bokota and Iskierka, 1995 did the same to transient problems. DeSilva et al., 1998, studied a transient formulation using transient fundamental solution. It showed that this BEM formulation presents low false diffusion. Xu and Zebib, 1996, showed a formulation for transient convection coupling the flow and the energy transport, using cell interpolation.

In the 2000s Hriberšek and Kuhn, 2000, solves heat transport between a solid and a Newtonian fluid, using velocity-vorticity formulation and cell integration. Grigoriev and Dargush, 2003a,b,c, showed formulation, implementation, and numerical results for 1D and 2D transient problems using cell interpolation to account for domain effects. Samec and Škerget, 2004, deals with advection-diffusion problems with first order chemical reaction using cell interpolation.

Ramirez Camacho and Barbosa, 2008, solves a steady-state energy transport coupled with Navier-Stokes forced convection problem using cell domain interpolation. Gao et al., 2013, does the same for transient forced convection problems.

Ravnik and Škerget, 2014, solves an advection-diffusion problem with variable coefficients, using both cell interpolation and sub-domain formulation. It concludes that the latter uses less memory and has numerical complexity of order $\mathcal{O}(N)$, while the former retains $\mathcal{O}(N^2)$ complexity.

2.2.2 Dual Reciprocity Methods

The dual reciprocity methodology was idealized and implemented by Nardini and Brebbia, 1983, to solve elastodynamics problems. It consists of expanding the domain terms on the integral equations into a series of functions depending on geometry and an unknown constant. These series of functions are usually simple radial based functions

with global support.

The use of DR methods for advection-diffusion problems began at the beginning of the '90s with Wrobel and DeFigueiredo, 1991a,b, showing the first formulations for, respectively, steady-state and transient problems. In the same decade, Partridge, 1994, studies the influence of local versus global interpolation in DR, while Zhu and Zhang, 1994, tried to improve the converge of certain domain integrals by using a transformation of the domain integral before the dual reciprocity scheme. By the end of the decade, Popov and Power, 1999, combines the DR technique with multi-domains. These proved to solve the convergence problems of the DR formulation for problems with high variations on the velocity field - in each sub-domain, the variation on the advective field is smaller, and the DR better represents the domain effects.

At the beginning of the 2000s, Rahaim et al., 2000; Blobner et al., 2000; Florez et al., 2002, studied formulations with multi-domain and dual reciprocity combined to solve Navier-Stokes coupled heat transport. Singh and Tanaka, 2003, used dual reciprocity to solve the transient part of a problem with constant coefficients. Rap et al., 2004, used the Laplace fundamental solution and dual reciprocity to solve the full advective and reaction terms in an advection-diffusion-reaction problem. The same author used a DR-BEM formulation to solve inverse source problems [Rap et al., 2006]. By the end of the decade, Bui and Popov, 2009a,b, presented papers using the combination of DR and subdomain to solve both steady-state and transient problems.

Bozkaya and Tezer-Sezgin, 2016, presented a DR-BEM formulation for a Navier-Stokes coupled, double-diffusion problem. In the same year, Chanthawara et al., 2016, published a study comparing the performance of shape functions used in the dual reciprocity formulation, for 2D steady-state problems using the Laplace fundamental solution. In the following year, Zakerdoost et al., 2017, showed a DR formulation for advection-diffusion-reaction problems using the Helmholtz fundamental solution and modeling the full advective terms using dual reciprocity. Chanthawara and Kaennakham, 2018, presented a DR-BEM study using locally supported radial basis functions with variable shape parameters. In the same year, AL-Bayati and Wrobel, 2018a, showed a study of DR-BEM for transient problems using different shape functions, and AL-Bayati and Wrobel, 2018b, showed an alternative formulation for transient problems using DR-BEM.

2.2.3 Sub-domain Boundary Element Methods

In a traditional boundary element formulation, the fundamental solution - as a globally supported function - connects every point in the problem with each other. That, by the end of the discretization process, gives rise to a fully populated, asymmetrical matrix, which has $\mathcal{O}(N^2)$ complexity.

One effort to bring the scheme to a $\mathcal{O}(N)$ complexity is the employment of domain subdivision. The sub-domains are treated traditionally, and they are connected to each other via compatibility conditions. This method effectively brings the complexity to $\mathcal{O}(N)$, but requires a *de facto* domain mesh, getting closer to a finite element scheme. It retains, however, characteristics like the improved convergence on dual variables and derivatives.

In the early 90s, Grigor'ev, 1994, used domain decomposition to solve a transport equation. In the same decade, Popov and Power, 1999, solved advective-diffusive problems using a Laplace fundamental solution and treats the domain effects using a combination of dual reciprocity and domain decomposition.

As mentioned before, Rahaim et al., 2000; Blobner et al., 2000; Florez et al., 2002, combined multi-domain and dual reciprocity to solve Navier-Stokes coupled heat transport. Portapila and Power, 2005, also used a combination of dual reciprocity and domain decomposition, and studied the influence of iteration methods and two different radial basis functions.

Thanh Tu and Popov, 2008 studied the use of overlapping sub-domains and dual reciprocity, using the Laplace fundamental solution. In the following year, Bui and Popov, 2009b and Bui and Popov, 2009a presented papers using the combination of DR and subdomain to solve both steady-state and transient problems.

In their presentation of the gradient-free BDIE to handle variable coefficient problems, Ravnik and Škerget, 2013 and Ravnik and Škerget, 2014 use domain decomposition on their solutions, as well as a single domain. They showed that the domain decomposition approach presents considerably lower memory usage and computational time for the same error. Ravnik et al., 2017 expands the formulation to one with coefficients that vary in space and time, as well as anisotropic diffusivity, and also used domain decomposition for the solution.

2.2.4 Radial Integration Methods

When the BEM is applied to non-linear problems or to problems that do not have a fundamental solution for the whole differential operator, we need to solve domain integrals. The radial integration boundary element method (RIBEM) is an approach, presented by Gao, 2002, that proposes a coordinate transformation of the domain integrals, using a radial integral and the boundary integral - the same one used for the boundary elements.

Gao, 2002, shows how this can be applied to deal with body forces using boundary-only discretization. When the domain integrals have unknown functions - such as the case for a variable coefficient equation - the unknown function needs to be interpolated in the domain. This interpolation is usually done by the use of radial basis interpolation functions.

Since this is a relatively new technique, we could not find many applications of it to advection-diffusion problems in BEM. AL-Bayati and Wrobel, 2019, shows the formulation for a problem where the only domain effect was a source. In the same year, Peng et al., 2019, showed a formulation for an advection-diffusion problem with variable coefficients.

2.3 Chapter Summary

In this chapter, we briefly reviewed the origins of integral equation methods and BEM. We followed by reviewing the first applications of it on linear scalar transport and how these applications augmented in scope over time. Special attention was paid on the most popular techniques for dealing with domain effects, namely cell integration, dual reciprocity, and domain decomposition, and also to a recent technique that has potential for expansion - the RIBEM.

3 INTEGRAL FORMULATION

In this chapter, we present the differential problem that is the target of this work and its associated fundamental solution. Using the weighted residuals technique, we deduce the inverse weighted residuals statement and the boundary-domain integral equation for this problem.

3.1 Differential Problem

The equation to be solved throughout this work will be the 2D, steady-state advection-diffusion-reaction equation with variable coefficients, presented below. This equation models the transport of a scalar property ϕ in a medium with constant specific mass and an incompressible velocity field.

$$\boldsymbol{v} \cdot \nabla\phi - \nabla \cdot (d\,\nabla\phi) + k\,\phi = S \tag{3.1}$$

where $\boldsymbol{v} : \Omega \to \mathbb{R}^2$ is the velocity field, $d : \Omega \to \mathbb{R}_{>0}$ is the diffusivity coefficient, that must also be differentiable in Ω, $k : \Omega \to \mathbb{R}$ is a linear source term, and $S : \Omega \to \mathbb{R}$ is an independent source term. All the coefficients are known, and none depends on the value of ϕ.

Equation 3.1 holds in the domain Ω, which is a connected subset of $\mathbb{R}^2$. The boundary of Ω is denoted by $\partial\Omega = \overline{\Omega} \setminus \Omega$. Let $\partial\Omega_D$ be the part of the boundary with Dirichlet boundary condition and $\partial\Omega_N$ be the part with Neumann boundary condition, then in a well-posed problem, we have $\partial\Omega = \partial\Omega_D \cup \partial\Omega_N$, $\partial\Omega_D \cap \partial\Omega_N = \varnothing$, and $\partial\Omega_D \neq \varnothing$. Meaning, respectively, that we have a boundary condition everywhere on the boundary, that we have either a Dirichlet or a Neumann condition in a given point, and that we have a Dirichlet condition somewhere on the boundary.

3.2 Weighted Residual Statement

There are many ways of getting the integral equations used in BEM from a given differential problem. Cheng and Cheng, 2005, shows the historical development of the boundary element method and the early use of integral equations. For potential problems, modeled by the Laplace equation, for example, the use of Green's identity will suffice. However, for non-linear problems, the derivation of the integral equations is not as direct.

In this work, we use the weighted residual method (WRM) to derive these equations due to its generality and wide range of applications [Brebbia and Dominguez, 1992].

When working with an approximate solution, by applying the differential operator to that approximation, we will have, in general, a non-null residual. Let us consider now the inner product between that residual R and a given weighting function ϕ^*.

$$< R,\, \phi^* >= \int_\Omega \phi^* \left(\boldsymbol{v} \cdot \nabla\phi - \nabla \cdot (d\,\nabla\phi) + k\,\phi - S\right) \mathrm{d}A \tag{3.2}$$

One way to search for the best possible approximation for a given approximation space is to make the residual of that approximation orthogonal to the approximation space. In other words, to make the inner product given in Equation 3.2 equal to zero.

$$\int_\Omega \phi^* \left(\boldsymbol{v} \cdot \nabla\phi - \nabla \cdot (d\,\nabla\phi) + k\,\phi - S\right) \mathrm{d}A = 0 \tag{3.3}$$

The integral statement in Equation 3.3 can be rewritten in different ways, and thus leading to different numerical methods. The BEM is derived from the inverse statement, where we integrate by parts the weighted residual expression in such a way that the differential operators are entirely applied to the weighting function.

We begin by rewriting the first term of the integral using the following relation:

$$\nabla \cdot (\boldsymbol{v}\,\phi\,\phi^*) = \nabla \cdot \boldsymbol{v}\ (\phi\,\phi^*) + \phi\,\boldsymbol{v} \cdot \nabla\phi^* + \phi^*\,\boldsymbol{v} \cdot \nabla\phi \tag{3.4}$$

Using the relation above and taking into account that the velocity field is incompressible, *i.e.* $\nabla \cdot \boldsymbol{v} = 0$, the first term in Equation 3.3 is written as:

$$\int_\Omega \phi^*\,\boldsymbol{v} \cdot \nabla\phi\,\mathrm{d}A = \int_\Omega \nabla \cdot (\boldsymbol{v}\,\phi\,\phi^*)\,\mathrm{d}A - \int_\Omega \phi\,\boldsymbol{v} \cdot \nabla\phi^*\,\mathrm{d}A \tag{3.5}$$

Applying the divergence theorem to the first integral on the right hand side:

$$\int_\Omega \phi^*\,\boldsymbol{v} \cdot \nabla\phi\,\mathrm{d}A = \int_{\partial\Omega} \phi\,\phi^*\,v_n\,\mathrm{d}l - \int_\Omega \phi\,\boldsymbol{v} \cdot \nabla\phi^*\,\mathrm{d}A \tag{3.6}$$

where v_n is the velocity normal to the boundary, *i.e.* $v_n = \boldsymbol{v} \cdot \boldsymbol{n}$.

The second term in Equation 3.3 is rewritten using the second Green identity:

$$-\int_\Omega \phi^*\,\nabla \cdot (d\,\nabla\phi)\,\mathrm{d}A = \int_{\partial\Omega} \phi\,d\,q^*\,\mathrm{d}l - \int_{\partial\Omega} q_n\,d\,\phi^*\,\mathrm{d}l - \int_\Omega \phi\,\nabla \cdot (d\,\nabla\phi^*)\,\mathrm{d}A \tag{3.7}$$

where $q_n = \nabla\phi \cdot \boldsymbol{n}$ and $q^* = \nabla\phi^* \cdot \boldsymbol{n}$ are the derivatives outward normal to the boundary of ϕ and ϕ^*, respectively.

Replacing Equations 3.6 and 3.7 into Equation 3.3 we get the inverse weighted residuals statement:

$$\int_{\Omega} \phi \left[-\boldsymbol{v} \cdot \nabla\phi^* - \nabla \cdot (d\,\nabla\phi^*) + k\,\phi^*\right] \mathrm{d}A + \int_{\partial\Omega} \phi\ (v_n\,\phi^* + d\,q^*)\ \mathrm{d}l + \\ - \int_{\partial\Omega} q_n\,d\,\phi^*\,\mathrm{d}l = \int_{\Omega} S\phi^*\,\mathrm{d}A \quad (3.8)$$

If a fundamental solution exists for the operator, we can choose a weighting function in such a way that the domain integral on the left side of Equation 3.8 vanishes due to the filtering property of the Dirac's delta distribution. In the next section, we will present the fundamental solution for the steady advection-diffusion-reaction operator with constant coefficients.

3.3 The Fundamental Solution

The fundamental solution ϕ^* for a linear differential operator L is the solution of the inhomogeneous equation below, in an infinite domain and with the derivatives of ϕ^* approaching zero as the distance to the origin tends to infinity.

$$L\,\phi^* = \delta_0 \quad (3.9)$$

where δ_0 is the Dirac's delta distribution placed at the origin.

The Malgrange–Ehrenpreis theorem [Malgrange, 1956; Ehrenpreis, 1955] states that every linear operator with constant coefficients has a fundamental solution. The same cannot be said if the operator has variable coefficients. The operator that we are using in this work is one with variable coefficients, meaning that we cannot assume that we will know a fundamental solution compatible with it.

Let $\boldsymbol{v}_\xi$, d_ξ, and k_ξ be the velocity, the diffusivity, and the linear reaction term, all constant. In this work, we will use the coefficients at some point $\boldsymbol{\xi} \in \overline{\Omega}$ as the values for the fundamental solution. Let us consider as well δ_ξ as Dirac's delta distribution centered at the same point. We will refer to this point $\boldsymbol{\xi}$ as the source point. Therefore, the fundamental solution ϕ^*_ξ for the source placed at $\boldsymbol{\xi}$ will be the solution to:

$$\boldsymbol{v}_\xi \cdot \nabla\phi^*_\xi + d_\xi\,\nabla^2\phi^*_\xi - k_\xi\,\phi^*_\xi = -\delta_\xi \quad (3.10)$$

with the derivatives of ϕ^*_ξ tending to zero when the distance from $\boldsymbol{\xi}$ tends to infinity. The

solution of Equation 3.10 exists as a real function only for values of $k_\xi > -v_\xi^2/4d_\xi$. In the scope of this work, we will consider only real-valued fundamental solutions. Due to this restriction we choose to include in the fundamental solution a linear annihilation term ($k > 0$) and to consider a linear generation term ($k < 0$) as variable domain contribution to be treated as a source. Then k_ξ is defined as:

$$k_\xi = max\left\{k(\xi), 0\right\} \tag{3.11}$$

We also define an auxiliary variable μ:

$$\mu = \sqrt{\left(\frac{v_\xi}{2d_\xi}\right)^2 + \frac{k_\xi}{d_\xi}} \tag{3.12}$$

The solution to Equation 3.10 is given by:

$$\phi_\xi^* = \begin{cases} \frac{-1}{2\pi d_\xi} \ln r & \text{for } \mu = 0 \\ \frac{1}{2\pi d_\xi} \mathrm{K}_0(\mu r) & \text{for } \mu \neq 0,\ v_\xi = 0 \\ \frac{1}{2\pi d_\xi} \exp\left(-\frac{\boldsymbol{v_\xi} \cdot \boldsymbol{r}}{2d_\xi}\right) \mathrm{K}_0(\mu r) & \text{for } \mu \neq 0,\ v_\xi \neq 0 \end{cases} \tag{3.13}$$

where $\boldsymbol{r}$ is the distance to the source point, r is the norm of said distance, and K_ν is the modified Bessel function of the second kind and order ν. It is worth noticing that the first and second cases correspond to Equation 3.10 in a degenerated form, with the velocity being zero.

The fundamental solution in the third case (with a non-null advective term) may present numerical instabilities. The Bessel function decreases rapidly with the increase of its argument, and due to its implementation, it loses accuracy for high values of the argument [MATLAB, 2018]. Matlab suggests the use of a scaled version of the Bessel function, shown below as K_ν^*, to improve accuracy in these cases. This increase in accuracy in itself does not provide significant improvements for the method, because the relative importance of values around the singularity is much higher than for values that are further away from it.

$$\mathrm{K}_\nu^*(x) = \exp(x)\mathrm{K}_\nu(x) \tag{3.14}$$

However, in some cases the scalar product $\boldsymbol{v_\xi} \cdot \boldsymbol{r}$ may be a large negative number, causing the argument of the exponential to be a large positive number and risking numerical overflow when calculating the fundamental solution. Considering that μ is in the

same order of magnitude as $v_\xi/2d_\xi$, and γ being the angle between the velocity and the radius vectors, the aforementioned scalar product will be of the same order as $\mu r \cos\gamma$. We can use this associated with the scaled Bessel function to rewrite the product as:

$$\exp\left(-\frac{\boldsymbol{v}_\xi \cdot \boldsymbol{r}}{2d_\xi}\right) \mathrm{K}_0(\mu r) = \exp\left(-\frac{\boldsymbol{v}_\xi \cdot \boldsymbol{r}}{2d_\xi} - \mu r\right) \mathrm{K}_0^*(\mu r) \tag{3.15}$$

In this case, the argument of the exponential will be either a large negative number or at most of order $\mathcal{O}(1)$, causing no numerical overflow in its evaluation. A numerically stable fundamental solution under the aforementioned conditions is written as:

$$\phi_\xi^* = \begin{cases} \frac{-1}{2\pi d_\xi} \ln r & \text{for } \mu = 0 \\ \frac{1}{2\pi d_\xi} \exp(-\mu r)\, \mathrm{K}_0^*(\mu r) & \text{for } \mu \neq 0,\ v_\xi = 0 \\ \frac{1}{2\pi d_\xi} \exp\left(-\frac{\boldsymbol{v}_\xi \cdot \boldsymbol{r}}{2d_\xi} - \mu r\right) \mathrm{K}_0^*(\mu r) & \text{for } \mu \neq 0,\ v_\xi \neq 0 \end{cases} \tag{3.16}$$

Figure 3.1a shows ϕ_ξ^* when the velocity is zero. In this case, the fundamental solution has radial symmetry. Figure 3.1b shows ϕ_ξ^* with velocity in the negative x-direction. In this case, the fundamental solution no longer has radial symmetry. This asymmetry becomes more significant the larger the absolute velocity is. For problems with very high Péclet numbers [Qiu et al., 1998] suggests an algorithm so simplify the BEM coefficient evaluations taking into account that in certain directions, the fundamental solution goes to zero rapidly.

We are interested in using the fundamental solution as a weighting function, and as can be seen in Equation 3.8, we need to use the gradient of ϕ^* to compute q^*. The derivative of the fundamental solution in a given direction $\boldsymbol{n}$ is:

$$\frac{\partial \phi_\xi^*}{\partial \boldsymbol{n}} = \begin{cases} \frac{-1}{2\pi d_\xi} \frac{r_n}{r^2} & \text{for } \mu = 0 \\ \frac{-\mu}{2\pi d_\xi} \frac{r_n}{r} \exp(-\mu r)\, \mathrm{K}_1^*(\mu r) & \text{for } \mu \neq 0,\ v_\xi = 0 \\ \frac{1}{2\pi d_\xi} \exp\left(-\frac{\boldsymbol{v}_\xi \cdot \boldsymbol{r}}{2d_\xi} - \mu r\right) \left[-\mu \mathrm{K}_1^*(\mu r) \frac{r_n}{r} - \frac{\boldsymbol{v}_\xi \cdot \boldsymbol{n}}{2d_\xi} \mathrm{K}_0^*(\mu r)\right] & \text{for } \mu \neq 0,\ v_\xi \neq 0 \end{cases} \tag{3.17}$$

3.4 The Boundary-Domain Integral Equation

Equation 3.8 will be rewritten while taking into account the properties of the fundamental solution in Equation 3.16. The first step is to separate the fields in the domain integral of the inverse statement into constant and perturbation parts. The first domain integral will disappear due to the properties of the delta distribution. The latter

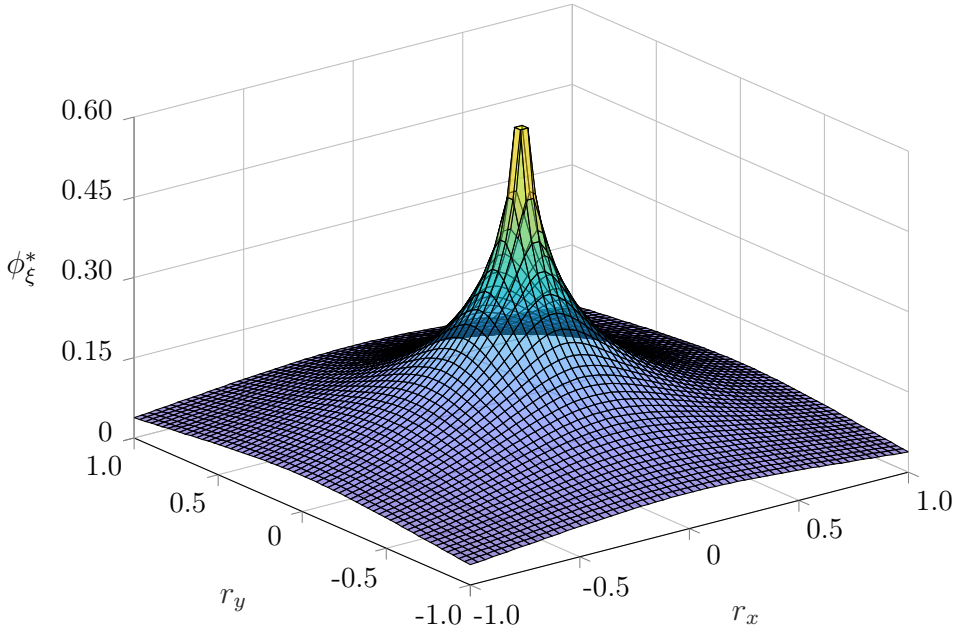

(a) ϕ^*_ξ with $\xi = 0$, $d_\xi = 1$, $k_\xi = 1$, $\boldsymbol{v}_\xi = (0, 0)$.

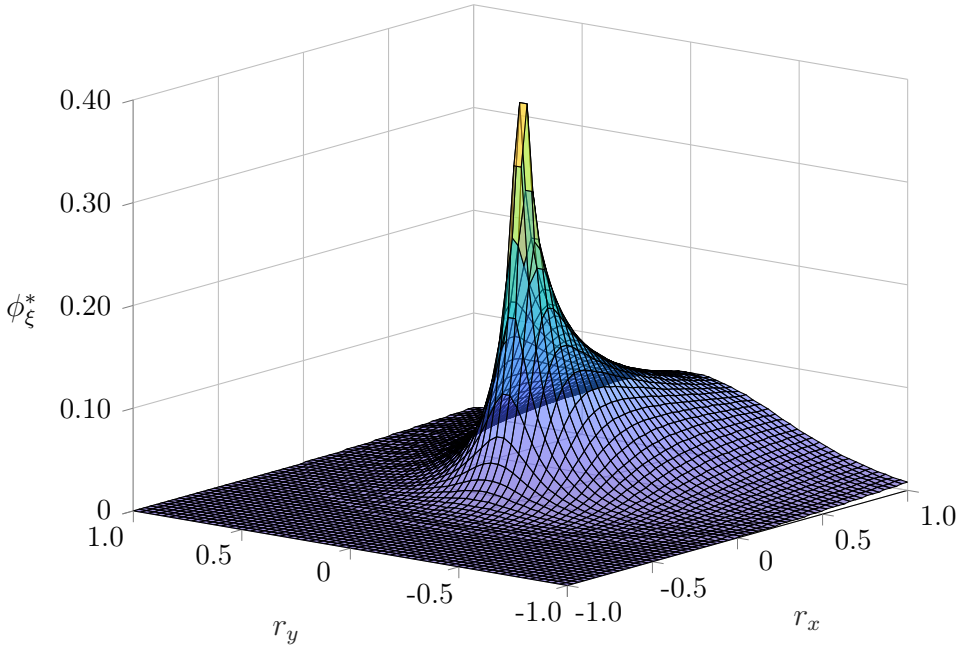

(b) ϕ^*_ξ with $\xi = 0$, $d_\xi = 1$, $k_\xi = 1$, $\boldsymbol{v}_\xi = (-10, 0)$.

Figure 3.1 – Fundamental solution plot. (a) A case where the velocity field is null. (b) A case where there is a velocity field present.

will be treated as a source term.

$$c_\xi\,\phi_\xi + \int_{\partial\Omega} \phi\,\left(v_n\,\phi^*_\xi + d\,q^*_\xi\right)\,\mathrm{d}l\; - \int_{\partial\Omega} q_n\,d\,\phi^*_\xi\,\mathrm{d}l\; = \int_\Omega S\phi^*_\xi \mathrm{d}A + \\ + \int_\Omega \phi\left[(\boldsymbol{v}-\boldsymbol{v}_\xi)\cdot\nabla\phi^*_\xi + \nabla\cdot((d-d_\xi)\nabla\phi^*_\xi) - (k-k_\xi)\,\phi^*_\xi\right]\mathrm{d}A \quad (3.18)$$

where c_ξ is a coefficient that depends on the location of the source point. For applications with the source point in the domain Ω it follows directly that $c_\xi = 1$, and if the source point is outside of Ω then $c_\xi = 0$. For a source point located in $\partial\Omega$ the value of c_ξ can be found using the trace property of the equation, expanding the domain by a semi-circle around the source point and making its radius tend to zero. The full expression for c_ξ is:

$$c_\xi = \begin{cases} 0 & \text{for } \boldsymbol{\xi} \notin \Omega \\ 1 & \text{for } \boldsymbol{\xi} \in \Omega \\ \frac{\theta}{2\pi} & \text{for } \boldsymbol{\xi} \in \partial\Omega \end{cases} \quad (3.19)$$

where θ is the internal angle of $\partial\Omega$ at the point $\boldsymbol{\xi}$. In a case where the boundary is smooth at $\boldsymbol{\xi}$ then $c_\xi = 1/2$.

The first boundary integral in Equation 3.18 contains a kernel with a combination of strong and weak singularities and must be interpreted in the Cauchy Principal Value (CPV) sense. The second boundary integral contains a kernel with a weak singularity, which is integrable in the classical sense.

The term corresponding to the perturbation of the diffusivity coefficient contains the Laplacian of the fundamental solution, and it can be rewritten using Equation 3.10:

$$\int_\Omega \phi\,\nabla\cdot((d-d_\xi)\nabla\phi^*)\,\mathrm{d}A = \int_\Omega \phi\left[\nabla d\cdot\nabla\phi^* + \right. \\ \left. + \frac{(d-d_\xi)}{d_\xi}(-\delta_\xi + k_\xi\,\phi^*_\xi - \boldsymbol{v}_\xi\cdot\nabla\phi^*_\xi)\right]\mathrm{d}A \quad (3.20)$$

At the source point $\boldsymbol{\xi}$, the perturbation on the diffusivity field tends to zero, since we are taking its value at the source point as the coefficient to be used on the fundamental solution. Therefore, in Equation 3.20, the term with the delta distribution vanishes. If we did not take that approach, the constant multiplying the free term ϕ_ξ on the BDIE would depend on the value of d/d_ξ, which could cause bad conditioning for the resulting system of equations. Ravnik and Škerget, 2013, and Ravnik and Škerget, 2014, use a similar procedure for their formulation, without considering a linear reaction term. Also,

these authors separate the weighted residuals statement in a constant-coefficient and a perturbation part in Equation 3.3, while in this work, we write the inverse statement with variable coefficients and do that separation afterward. Replacing Equation 3.20 on Equation 3.18, we get the final form of the BDIE:

$$c_\xi\,\phi_\xi + \int_{\partial\Omega} \phi\,\left(v_n\,\phi^*_\xi + d\,q^*_\xi\right)\,\mathrm{d}l\; - \int_{\partial\Omega} q_n\,d\,\phi^*_\xi\,\mathrm{d}l\; = \int_\Omega S\phi^*_\xi \mathrm{d}A + \\ + \int_\Omega \phi\,\left[\left(\boldsymbol{v} - \frac{d}{d_\xi}\boldsymbol{v}_\xi + \nabla d\right)\cdot\nabla\phi^*_\xi + \left(\frac{d}{d_\xi}k_\xi - k\right)\phi^*_\xi\right]\mathrm{d}A \quad (3.21)$$

The domain term in Equation 3.21 has a weak singularity and can be interpreted in the traditional sense. Notice that the integral of the derivatives of the fundamental solution around the singularity is possible in the classical sense for a two-dimensional integration domain, but must be interpreted in the CPV sense in a one-dimensional integration domain.

There are alternative versions of this integral equation. For example, [Wrobel and DeFigueiredo, 1991a; AL-Bayati and Wrobel, 2018a,b], use a version of the BDIE with the gradient of the unknown ϕ in the domain integral, treating said integral with the dual reciprocity BEM. We will use domain cells to deal with the domain terms in Equation 3.21, and the integral equation will be applied to internal nodes as well as boundary nodes. As shown by Ravnik and Škerget, 2013, and Ravnik and Škerget, 2014, we would either have to interpolate ϕ and calculate its gradient by derivating the interpolation functions with loss of precision and need of an iterative process, or we would have to apply integral equations for the derivatives of ϕ in the internal points, doubling the number of equations for these points and having a CVP integral on the domain. For these reasons, a gradient-free version of the BDIE is preferable.

3.5 Analytical treatment of point sources in the domain

In some transport problems, it is useful to model sources as a Dirac delta distribution. For example, when considering pollutant transport due to the discharge of an industrial complex on the atmospheric boundary layer, the dimensions of said tower are much smaller than the ones involving the considered domain, and it is useful to represent it as a point discharge. Let us consider the case where the source S can be divided into a

continuous distribution in the domain and a sum of point sources of different strengths:

$$S = S_f + \sum_{k=1}^{n_k} s_k \delta_{\boldsymbol{x}_k} \tag{3.22}$$

where S_f is the limited part of the domain source, n_k is the number of point sources, s_k is the strength of the k-th point source, and $\boldsymbol{x}_k \in \Omega$ is its location. We can use Equation 3.22 to rewrite the source term in Equation 3.21 using the filtering property of the delta distributions.

$$\int_\Omega S\phi^*_\xi \mathrm{d}A = \int_\Omega S_f\, \phi^*_\xi \mathrm{d}A + \sum_{k=1}^{n_k} s_k\, \phi^*_\xi(\boldsymbol{x}_k) \tag{3.23}$$

In this way, the influence of point sources can be computed by the evaluation of the fundamental solution on their respective locations, without the need for local mesh refinement as we would in a domain method such as the finite volume or the finite element methods. The integral equation cannot be evaluated for the $\boldsymbol{x}_k$ points, since ϕ is not defined for them. Therefore, nodes for the domain cells cannot be placed at these locations.

3.6 Derivatives at interior points

One may be interested in calculating the value of the derivatives of ϕ in some point of Ω. On the finite volume method that could be done by finite difference. On the finite element method, this is done by directional differentiation of the interpolation functions of the given element. Derivatives at internal points using BEM can be done in different ways.

$$\left.\frac{\partial \phi}{\partial x}\right|_\xi = \lim_{h\to 0} \frac{\phi(\xi + h) - \phi(\xi)}{h} \tag{3.24}$$

Equation 3.24 is the definition of a derivative. One could apply the BDIE in two points very close to each other, and approximate the derivative by a finite difference scheme. There are two drawbacks to this approach: there would be the need to calculate the integral equation twice, and there would be some loss of precision due to the finite

difference scheme.

$$\left.\frac{\partial\phi}{\partial x}\right|_{\xi} = \lim_{h\to 0}\left\{ -\int_{\partial\Omega}\phi\left(v_n\,\frac{\phi^*_{\xi+h}-\phi^*_{\xi}}{h} + d\,\frac{q^*_{\xi+h}-q^*_{\xi}}{h}\right)\mathrm{d}l + \int_{\partial\Omega} q_n\,d\,\frac{\phi^*_{\xi+h}-\phi^*_{\xi}}{h}\,\mathrm{d}l + \right.$$
$$+\int_{\Omega} S\frac{\phi^*_{\xi+h}-\phi^*_{\xi}}{h}\mathrm{d}A + \int_{\Omega}\phi\left[\left(\boldsymbol{v} - \frac{d}{d_\xi}\boldsymbol{v}_\xi + \nabla d\right)\cdot\nabla\left(\frac{\phi^*_{\xi+h}-\phi^*_{\xi}}{h}\right) + \right.$$
$$\left.\left.+\left(\frac{d}{d_\xi}k_\xi - k\right)\frac{\phi^*_{\xi+h}-\phi^*_{\xi}}{h}\right]\mathrm{d}A\right\} \quad (3.25)$$

The other approach would be to analytically manipulate this limit. Equation 3.25 shows the limit with the integral equations for the source points ξ and $\xi + h$ explicitly written. Due to the characteristics of the kernels to be integrated, the limit can be passed to the inside of the integrals. The value of ϕ and q_n do not change with the placement of the source point, nor do the variable coefficients. The only terms that depend on that placement are the fundamental solution and its derivatives. Thus, the limit can be directly applied to these terms, resulting in:

$$\left.\frac{\partial\phi}{\partial x}\right|_{\xi} = -\int_{\partial\Omega}\phi\left(v_n\,\frac{\partial\phi^*_{\xi}}{\partial x} + d\,\frac{\partial q^*_{\xi}}{\partial x}\right)\mathrm{d}l + \int_{\partial\Omega} q_n\,d\,\frac{\partial\phi^*_{\xi}}{\partial x}\,\mathrm{d}l + \int_{\Omega} S\frac{\partial\phi^*_{\xi}}{\partial x}\mathrm{d}A +$$
$$+\int_{\Omega}\phi\left[\left(\boldsymbol{v} - \frac{d}{d_\xi}\boldsymbol{v}_\xi + \nabla d\right)\cdot\frac{\partial}{\partial x}\nabla\phi^*_{\xi} + \left(\frac{d}{d_\xi}k_\xi - k\right)\frac{\partial\phi^*_{\xi}}{\partial x}\right]\mathrm{d}A \quad (3.26)$$

In Equation 3.26 the boundary integrals are regular since the source point is inside the domain. The domain integral has a strong singularity and must be interpreted in the CPV sense. The increase in the singularity order is one of the drawbacks of this approach in problems with domain integrals. Also, when the source point is close to the boundary, but not directly in it, the boundary integrals are technically regular, but they have high gradients that are difficult to integrate with numerical schemes. When calculating internal values at points that are critically close to the boundary, special care must be taken to perform the integrals.

The added complexity of the integrals on Equation 3.26 is one of the reasons why a BDIE formulation is preferable instead of a BDIDE. To generate equations for the unknowns of the derivatives of ϕ would rely on the solution on strongly singular integrals for the domain nodes. Moreover, these would come in addition to the equations for ϕ on the domain nodes, as they would still be needed.

3.7 Chapter Summary

This chapter stated the differential problem to be tackled in this work. We also deduced the weighted residuals inverse statement for the problem. The fundamental solution was presented, and a numerically stable form of it was introduced to be used instead of the traditional one. We deduced the gradient-free form of BDIE that will be used in the implementation of the BEM that can handle degenerated forms of the equation as is. We also showed the analytical treatment of point sources and the integral equation for derivatives.

4 NUMERICAL IMPLEMENTATION

In this chapter, we will discuss the numerical implementation of a BEM code based on the BDIE shown in Equation 3.21. We will talk about the discretization of the equation based on compact support polynomials. It will be followed by the collocation process and the assembly of the linear system to be solved. Moreover, we will discuss numerical integration, showing the utilized schemes and their convergence for chosen critical cases.

4.1 Discretization

The 1D geometry and variables, namely the boundary itself and the boundary values of ϕ and q_n, are interpolated using continuous linear finite elements everywhere except at points where the boundary is not smooth, or a boundary condition discontinuity is present. These variables are represented in discrete form as:

$$u(\boldsymbol{x}) = \sum_{j=1}^{n_j} u_j \psi_j(\boldsymbol{x}) \tag{4.1}$$

where n_j is the number of boundary nodes, u is the variable to be interpolated, namely x, y, ϕ, or q_n, u_j is its value at the node j, and ψ_j is the compact support 1D shape function corresponding to the node j. The three sets of shape functions for continuous and discontinuous elements are shown in Appendix A.

We need to treat corners differently because, at a point where the boundary is not smooth, we do not have a precise definition of a normal vector. At a corner point, we have normal vectors defined in two different directions, and, consequently, we cannot have a single value of q_n. By making a discontinuous interpolation at these points, we no longer have this problem. The discontinuous interpolation is not the only solution to the corner problem; other approaches are discussed in Brebbia and Dominguez [1992]; Chan and Chandra [1991].

That discretization implies that the boundary is approximated using line segments where the normal vector is constant, simplifying the numerical integration process. Also, when placing a source point on the nodes at the boundary, we have to take into account the angle formed by the elements. The coefficient c_ξ depends on the internal angle of the approximated boundary and should be calculated as such, even if the boundary is smooth.

Though the offset parameter in discontinuous elements can be chosen arbitrarily, Brebbia and Dominguez, 1992, shows that values close to 25% of the element's length give good results. We will use this value throughout all the cases studied.

Domain effects are computed using cell integration. The unknown ϕ in the domain is interpolated using discontinuous bilinear interpolation functions. The representation of such variables is:

$$u(\boldsymbol{x}) = \sum_{l=1}^{n_l} u_l \Psi_l(\boldsymbol{x}) \tag{4.2}$$

where n_l is the number of internal nodes, u is the variable to be interpolated, namely x, y, or ϕ, u_l is its value at the node l, and Ψ_l is the compact support 2D shape function corresponding to the node l. The set of shape functions used for the discontinuous cells are shown in Appendix A.

Replacing Equations 4.1 and 4.2 into Equation 3.21 we get the discretized integral equation, shown below. Since in each j boundary node we know either ϕ_j or q_{nj}, we will have $n_j + n_l + 1$ unknowns. In the next subsection, we will discuss the collocation process and the resulting linear system of equations.

$$c_\xi \, \phi_\xi + \sum_{j=1}^{n_j} \phi_j \int_{\partial\Omega} \psi_j \, \left(v_n \, \phi_\xi^* + d \, q_\xi^* \right) \, \mathrm{d}l \, - \sum_{j=1}^{n_j} q_{nj} \int_{\partial\Omega} \psi_j \, d \, \phi_\xi^* \, \mathrm{d}l \, = \int_\Omega S \phi_\xi^* \mathrm{d}A + \\ + \sum_{l=1}^{n_l} \phi_l \int_\Omega \Psi_l \left[\left(\boldsymbol{v} \, - \frac{d}{d_\xi} \boldsymbol{v}_\xi + \nabla d \right) \cdot \nabla \phi_\xi^* + \left(\frac{d}{d_\xi} k_\xi - k \right) \phi_\xi^* \right] \mathrm{d}A \tag{4.3}$$

4.2 Collocation and Resulting Matrix System

In the classical BEM, the system of equations is formed by the collocation process, where we apply the integral equation 3.21 with the source point coinciding with each node used for the interpolation.

For the j-th boundary node, $\phi_\xi = \phi_j$. Let ϕ^b and q_n^b be vectors containing the n_j boundary nodal values of ϕ and q_n. Also, let ϕ^d be a vector containing the nodal values of ϕ in each of the n_l internal nodes. By applying the fundamental solution with the singularity in each boundary node, we will then have the following n_j equations in matrix form:

$$\boldsymbol{H}^b \phi^b - \boldsymbol{G}^b q_n^b = \boldsymbol{B}^b \phi^d + \boldsymbol{b}^b \tag{4.4}$$

where $\boldsymbol{H}^b$ is the n_j-by-n_j coefficient matrix for the boundary values of ϕ, $\boldsymbol{G}^b$ is the n_j-by-

n_j coefficient matrix for the boundary values of q_n, $\boldsymbol{B}^b$ is the n_j-by-n_l coefficient matrix for the internal values of ϕ, and the $\boldsymbol{b}^b$ is a vector that contains the source influence, separated into point and domain sources as in Equation 3.22. Their components are defined by:

$$H_{ij}^b = \delta_{ij} c_i + \int_{\partial\Omega} \psi_j \, (v_n \, \phi_i^* + d \, q_i^*) \, \mathrm{d}l \tag{4.5}$$

$$G_{ij}^b = \int_{\partial\Omega} \psi_j \, d \, \phi_i^* \, \mathrm{d}l \tag{4.6}$$

$$B_{il}^b = \int_{\Omega} \Psi_l \left[\left(\boldsymbol{v} - \frac{d}{d_i} \boldsymbol{v}_i + \nabla d \right) \cdot \nabla \phi_i^* + \left(\frac{d}{d_i} k_i - k \right) \phi_i^* \right] \mathrm{d}A \tag{4.7}$$

$$b_i^b = \int_{\Omega} S_f \phi_i^* \mathrm{d}A + \sum_{k=1}^{n_s} s_k \phi_i^* (\boldsymbol{x}_k) \tag{4.8}$$

where δ_{ij} is the Kronecker's delta, and i is a given source point.

In the same way, by applying the fundamental solution with the singularity in each internal node, we will have the following n_l equations in matrix form:

$$\boldsymbol{H}^d \phi^b - \boldsymbol{G}^d q_n^b = \boldsymbol{B}^d \phi^d + \boldsymbol{b}^d \tag{4.9}$$

where $\boldsymbol{H}^d$ is the n_l-by-n_j coefficient matrix for the boundary values of ϕ, $\boldsymbol{G}^d$ is the n_l-by-n_j coefficient matrix for the boundary values of q_n, $\boldsymbol{B}^d$ is the n_l-by-n_l coefficient matrix for the internal values of ϕ, and the $\boldsymbol{b}^d$ is a vector that contains the source influence, separated into point and domain sources as in Equation 3.22. Their components are defined by:

$$H_{ij}^d = \int_{\partial\Omega} \psi_j \, (v_n \, \phi_i^* + d \, q_i^*) \, \mathrm{d}l \tag{4.10}$$

$$G_{ij}^d = \int_{\partial\Omega} \psi_j \, d \, \phi_i^* \, \mathrm{d}l \tag{4.11}$$

$$B_{il}^d = -\delta_{il} + \int_{\Omega} \Psi_l \left[\left(\boldsymbol{v} - \frac{d}{d_i} \boldsymbol{v}_i + \nabla d \right) \cdot \nabla \phi_i^* + \left(\frac{d}{d_i} k_i - k \right) \phi_i^* \right] \mathrm{d}A \tag{4.12}$$

$$b_i^d = \int_{\Omega} S_f \phi_i^* \mathrm{d}A + \sum_{k=1}^{n_s} s_k \phi_i^* (\boldsymbol{x}_k) \tag{4.13}$$

Since for every given source point at the boundary we know either ϕ or q_n, we will swap the columns of $\boldsymbol{H}^b$ and $\boldsymbol{G}^b$ in such a way that the columns corresponding to unknowns are placed at the left-hand side matrix, $\boldsymbol{A}^b$, while the other columns, together with the known values of boundary conditions, will form a vector $\boldsymbol{c}^b$. We form $\boldsymbol{A}^d$ and $\boldsymbol{c}^d$ for the internal source points in the same way. These matrices are assembled in a single

linear matrix system to be solved, shown below.

$$\begin{bmatrix} A^b & -B^b \\ A^d & -B^d \end{bmatrix} \begin{bmatrix} \chi^b \\ \phi^d \end{bmatrix} = \begin{bmatrix} b^b + c^b \\ b^d + c^d \end{bmatrix} \tag{4.14}$$

where χ^b is a vector containing the n_j unknowns at the boundary.

The code was implemented using Matlab, and the system in Equation 4.14 is solved using Matlab's direct solver. Even though there is no fundamental solution for the advection-diffusion operator with known variable coefficients, the equation is still linear, and the system of equations thus defined can be solved directly. In cases where we have any coefficient varying as a function of ϕ the system will no longer be linear.

4.3 Numerical Integration

In order to assemble the matrix system, we need to calculate each component of $\boldsymbol{H}^b$, $\boldsymbol{G}^b$, $\boldsymbol{B}^b$, $\boldsymbol{b}^b$, $\boldsymbol{H}^d$, $\boldsymbol{G}^d$, $\boldsymbol{B}^d$, $\boldsymbol{b}^d$ by performing the integrals shown in Equations 4.5 to 4.8. The fundamental solution has global support; however, the shape functions ψ_j and Ψ_l have compact support. Therefore, the integration can be performed one element (or cell) at the time. All the integrations will be performed in the normalized space used to define the shape functions. Since our one-dimensional elements are linear, their Jacobian is constant over the integration domain. The same cannot be said for the bilinear domain cells.

4.3.1 Qualitative behavior of the kernels

The behavior of the kernels in Equations 4.5 to 4.8 vary radically depending on the source location and on which element (or cell) is being integrated. When the source point is located in the domain to be integrated, then the kernel is singular. Otherwise, it is regular. As shown by Qiu et al., 1998 the asymptotic behavior of the singular terms presented in Equations 3.16 and 3.17 as $r \to 0$ is:

$$\mathrm{K}_0(\mu r) = -\ln\frac{\mu r}{2} + \mathcal{O}(1) \tag{4.15}$$

$$\exp\left(-\frac{\boldsymbol{v}_\xi \cdot \boldsymbol{r}}{2d_\xi} - \mu r\right)\mathrm{K}_0^*(\mu r) = -\ln\frac{\mu r}{2} + \mathcal{O}(1) \tag{4.16}$$

$$\exp\left(-\frac{\boldsymbol{v}_\xi \cdot \boldsymbol{r}}{2d_\xi} - \mu r\right)\mu\mathrm{K}_1^*(\mu r)\frac{r_n}{r} = \frac{r_n}{r^2} + \mathcal{O}(1) \tag{4.17}$$

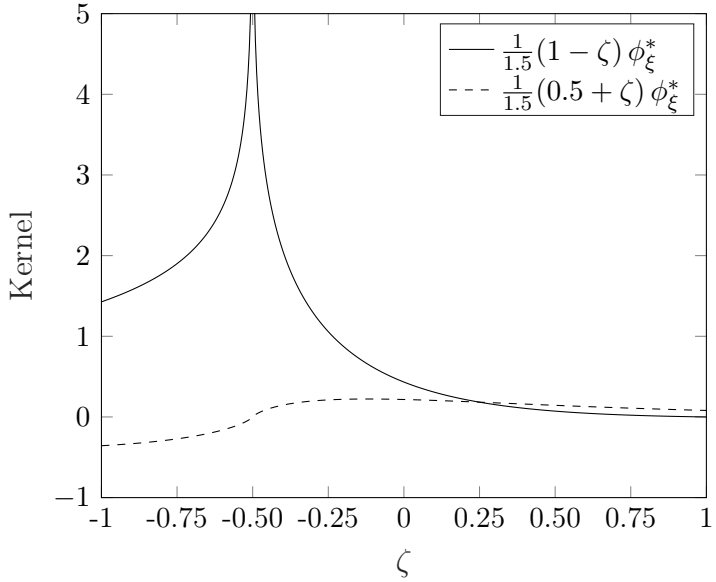

Figure 4.1 – Qualitative behavior of a weakly singular kernel present on the $\boldsymbol{G}^b$. The curves represent the fundamental solution with $\xi = -0.5$, $\boldsymbol{v}_\xi = (1, 0)$, $d_\xi = 1$, $k_\xi = 1$, when multiplied by a shape function either approaching 1 or 0 at the singularity point.

We start by analyzing the $\boldsymbol{G}^b$ terms. Singular kernels may arise when the source point is placed on the node corresponding to the shape function, or possibly to the nodes adjacent to it (in case of continuous elements). In the case when $i = j$ the shape function tends to 1 at the singularity point. In this case, the kernel is singular with the same asymptotic behavior as the fundamental solution. When we are integrating a kernel with a shape function that tends to zero at the singularity point, the resulting kernel is regular. Figure 4.1 shows the qualitative behavior of the fundamental solution when multiplied by a shape function - either approaching one or zero at the singularity point. Thus, only the diagonal terms of $\boldsymbol{G}^b$ will have singular kernels, and they will have the asymptotic behavior of a natural logarithm, and thus weakly singular in a one-dimensional integration domain.

$\boldsymbol{H}^b$ may have, *a priori*, a combination of strongly and weakly kernels to be integrated. The equation below shows the integrand of $\boldsymbol{H}^b$ with the fundamental solutions written explicitly and in the normalized space.

$$H^b_{ij} = \frac{J}{2\pi d_\xi}\int_{-1}^{1}(a_j\zeta + b_j)\left[\left(d_\xi \mu \mathrm{K}^*_1(\mu r)\frac{\boldsymbol{r}\cdot\boldsymbol{n}}{r} + \frac{v_n}{2}\mathrm{K}^*_0(\mu r)\right) + \right.$$
$$\left. + v_n \mathrm{K}^*_0(\mu r)\right]\exp\left(-\frac{\boldsymbol{v}_\xi\cdot\boldsymbol{r}}{2d_\xi} - \mu r\right)\mathrm{d}\zeta \quad (4.18)$$

where J is the Jacobian transformation, a_j and b_j are polynomial coefficients of ζ corresponding to ψ_j, and ζ is the normalized coordinate.

Since we are using linear elements, the scalar product $\boldsymbol{r} \cdot \boldsymbol{n}$ that multiplies the strongly singular term will be identically zero throughout the integration domain. That means it is necessary to calculate only the weakly singular terms, and they will have singular behavior only for the diagonal terms of $\boldsymbol{H}^b$.

When the source point is at the boundary, there will also appear a singularity on the domain cell that is immediately adjacent to that point. Therefore, a few of the $\boldsymbol{B}^b$ terms will have weak singularities, and, for the same reason, some of the cells used to calculate each term of $\boldsymbol{b}^b$ will also have weakly singular behavior.

Due to the use of $\alpha = 0.5$ as the discontinuity parameter for the cells and the fact that the cells are generally much bigger than the elements, no quasi-singular integral will appear when calculating the terms for $\boldsymbol{H}^d$ and $\boldsymbol{G}^d$. The internal nodes will be far enough from the boundary, allowing us to employ the classical Gauss-Legendre quadrature.

When the source point is in the domain, we will have a weak singularity inside one of the cells. For the same reason as before, when Ψ_l tends to zero at the singularity point, the kernel is regular. When Ψ_l tends to 1 at the singularity point, then the kernels will be weakly singular. That occurs for the diagonal terms of $\boldsymbol{B}^d$ and for one of the cells used to integrate $\boldsymbol{b}^d$ in the case of the presence of a distributed domain source. Notice that the derivatives of the fundamental solution form strongly singular kernels when integrated in a one-dimensional domain and weakly singular kernels for a two-dimensional domain.

Weakly singular integrals are integrable in the classical sense, meaning they do not form divergent kernels, and they could technically be evaluated using a traditional Gauss-Legendre quadrature. However, they would require a prohibitive number of integration points in order to have an acceptable degree of precision.

4.3.2 Cubic coordinate transformation

Many valid strategies could be used to compute the weakly singular kernels that appear in this work. We chose to use a cubic coordinate transformation, proposed by Telles, 1987. The idea behind this transformation is to use the points and weights from the Gauss-Legendre quadrature in a transformed space, where the Jacobian of this transformation is zero at the singularity point.

The transformation maps the interval $[-1, 1]$ onto itself. The resulting kernel, counting the Jacobian, will be regularized. For evaluating the integrals it suffices to calculate the kernel at the transformed points, and to transform the weighs accounting for the Jacobian of the transformation. Let φ be the cubic mapping, f be a generic kernel, x_g be the Gauss-Legendre quadrature points, and ω_g be the quadrature weights. Then the integral may be written as:

$$\int_{-1}^{1} f(\zeta)d\zeta \approx \sum_{g=1}^{n_g} \omega_g \, f(x_g) \approx \sum_{g=1}^{n_g} \omega_g \, \varphi'(x_g) \, f(\varphi(x_g)) \tag{4.19}$$

In this case, it is more convenient to use new points $x_t = \varphi(x_g)$ and new weighs $\omega_t = \omega_g \varphi'(x_g)$ and compute this quadrature in the same manner as we would a Gauss-Legendre one. Expressions for φ and φ' can be found in Appendix B.. The figure below shows, to the left, a weakly singular kernel with 20 x_g Gauss-Legendre point locations, and, to the right, the kernel applied to the transformed variable and the location of the transformed quadrature points. The points become so close to each other near the singularity ($\zeta = 0$) that it is hard to distinguish them in the figure.

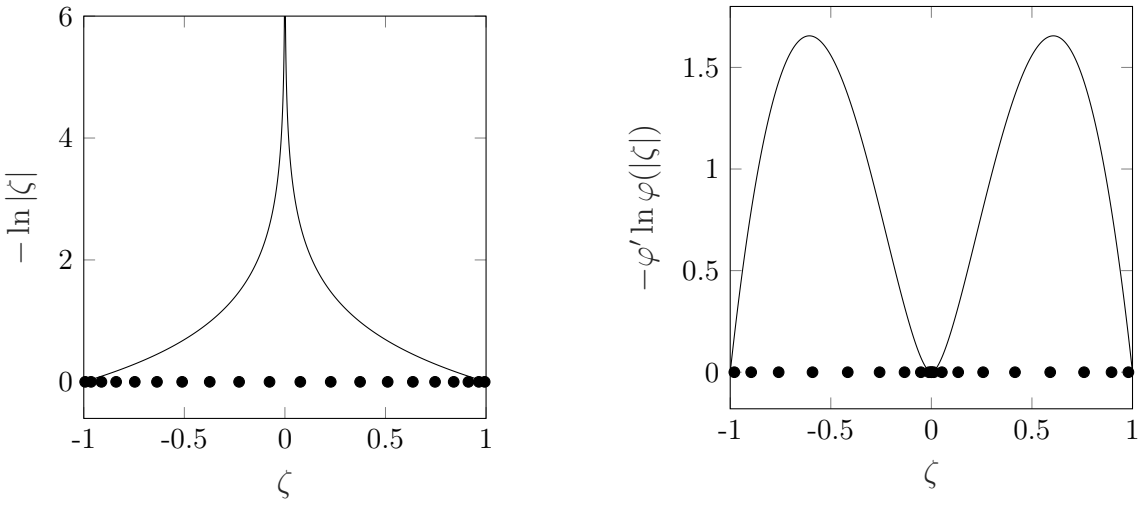

(a) Weakly singular kernel $-\ln|\zeta|$ and 20 x_g.

(b) Regularized kernel $-\varphi' \ln \varphi|\zeta|$ and 20 x_t.

Figure 4.2 – (a) Weakly singular kernel and Gauss-Legendre quadrature points. (b) Regularized kernel using Telles' transformation and the new quadrature points.

For two dimensional integrals, the transformation is done on the two directions,

centered on the singularity point. This transformation could also be used to improve integration performance of functions that have high variation at some point in their domain, since it concentrates the evaluation points near this region of high complexity. We will use this coordinate transformation not only for the weakly singular kernels but also for the kernels that are regularized by the shape function of a given element.

4.3.3 Study of quadrature order

The kernels to be integrated are varied, and it is necessary to choose an adequate number of integration points for each case. In order to estimate that number, we will use a fictitious kernel that has the complexity of the harder case to integrate in each type of element. The metric used to assess the quality of the integrations is the relative absolute deviation in relation to a numerical integration performed by the software Maple [Maplesoft, a division of Waterloo Maple Inc., 2011] with ten significant digits.

We will begin by examining a regular integral in a boundary element, given by I_1 (defined below). In this case the source is at $\zeta = -1.5$, and we have a fundamental solution with $\boldsymbol{v}_\xi = (-1, 0)$, $d_\xi = 1$, and $k_\xi = 1$. We use the shape function for the node $\zeta = -1$.

$$I_1 = \int_{-1}^{1} (1 - \zeta) \exp\left(\frac{\zeta + 1.5}{2}\right) \mathrm{K}_0(\mu|\zeta + 1.5|)\mathrm{d}\zeta \tag{4.20}$$

As we can see in Figure 4.3 this integral can be solved by the Gauss-Legendre quadrature with a relatively small number of points. We chose to use 12 points for these integrals.

In Figure 4.4 we will examine kernels where the source is at one end of a boundary element, given by I_{2a} and I_{2b}. The source is at $\zeta = -1$, and we have a fundamental solution with $\boldsymbol{v}_\xi = (-1, 0)$, $d_\xi = 1$, and $k_\xi = 1$. In I_{2a} we have a shape function approaching 2 at the singularity point, and in I_{2b} we have a shape function approaching zero at that point.

$$I_{2a} = \int_{-1}^{1} (1 - \zeta) \exp\left(\frac{\zeta + 1}{2}\right) \mathrm{K}_0(\mu|\zeta + 1|)\mathrm{d}\zeta \tag{4.21}$$

$$I_{2b} = \int_{-1}^{1} (1 + \zeta) \exp\left(\frac{\zeta + 1}{2}\right) \mathrm{K}_0(\mu|\zeta + 1|)\mathrm{d}\zeta \tag{4.22}$$

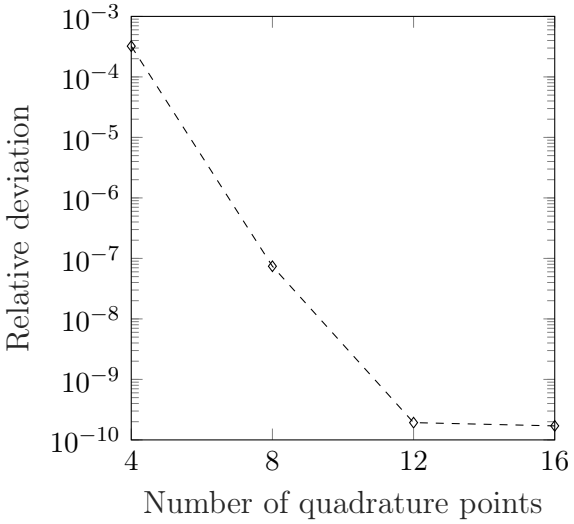

Figure 4.3 – Quadrature convergence for I_1.

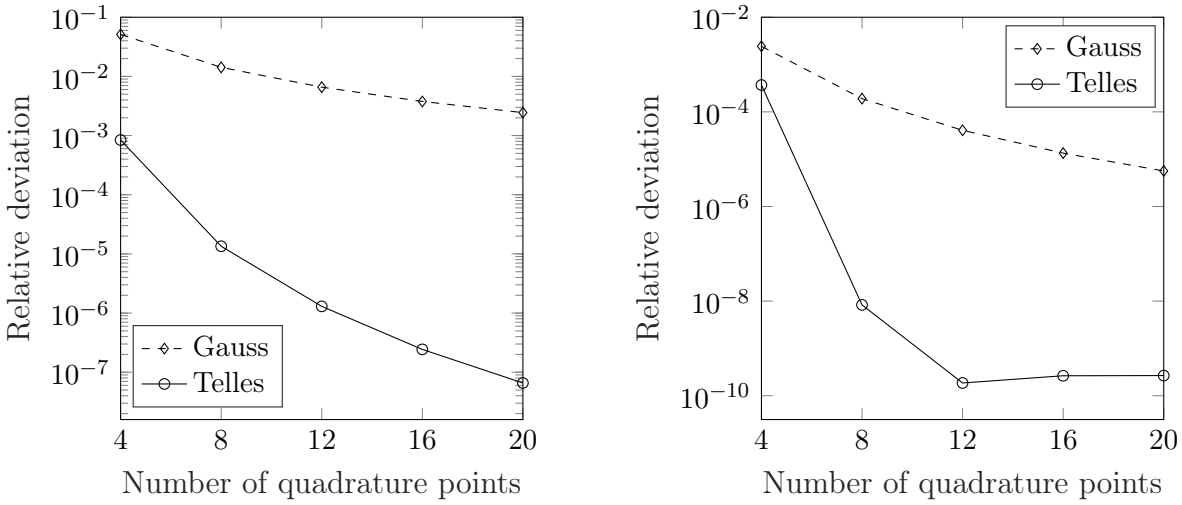

(a) Singular kernel

(b) Regularized by Ψ

Figure 4.4 – Quadrature convergence for (a) I_{2a} and (b) I_{2b}.

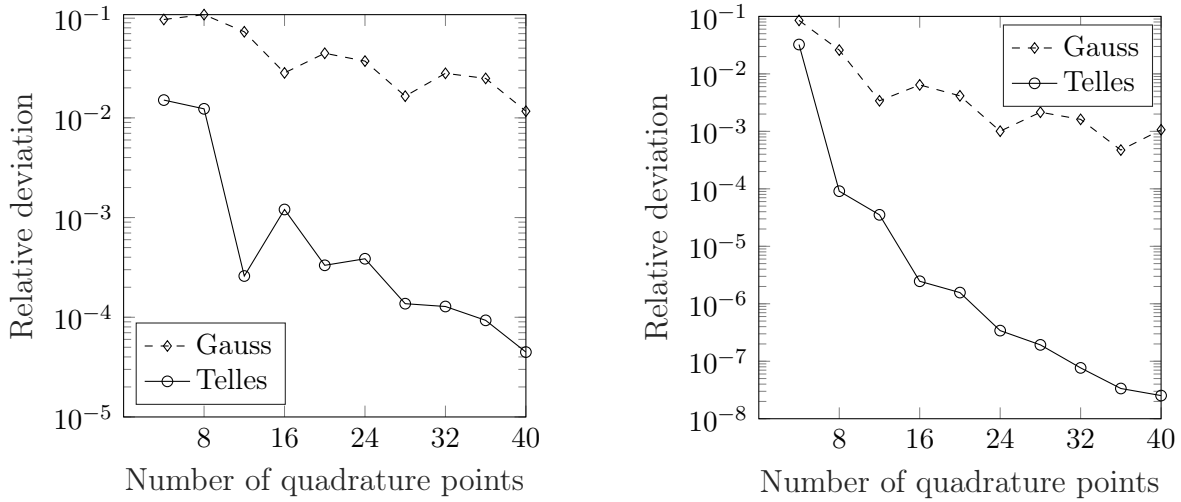

(a) Singular kernel

(b) Regularized by Ψ

Figure 4.5 – Quadrature convergence for (a) I_{3a} and (b) I_{3b}.

Figure 4.4 shows the performance of the two integration techniques, and it is clear that the Telles transformation should be used in both the singular kernel and the one that is regularized by the shape function. In these cases, we chose 16 points for their evaluation.

Our discretization has elements that are discontinuous at some points, such as corners, for example. In this case, the source point is at $\zeta = -0.5$, and the kernels are:

$$I_{3a} = \int_{-1}^{1} (1-\zeta) \exp\left(\frac{\zeta+0.5}{2}\right) \mathrm{K}_0(\mu|\zeta+0.5|)\mathrm{d}\zeta \tag{4.23}$$

$$I_{3b} = \int_{-1}^{1} (1+0.5\zeta) \exp\left(\frac{\zeta+0.5}{2}\right) \mathrm{K}_0(\mu|\zeta+0.5|)\mathrm{d}\zeta \tag{4.24}$$

Comparing Figures 4.5 and 4.4, we see that when the source point is inside the element, the integration becomes more difficult. In these cases, we chose to use 40 quadrature points.

The integral I_4 represents a regular kernel of a domain cell, with a source at $\zeta = -1.5$ and $\eta = 0$. In this case $r = \sqrt{(\zeta+1.5)^2 + \eta^2}$.

$$\Psi_{I4} = (1 + 2(\zeta+0.5) + 2(\eta+0.5) + 4(\zeta+0.5)(\eta+0.5)) \tag{4.25}$$

$$I_4 = \Psi_{I4} \exp\left(\frac{\zeta+1.5}{2}\right) \left[-\mu \mathrm{K}_1(\mu r)\frac{\zeta+1.5}{r} - 0.5\mathrm{K}_0(\mu r)\right] \tag{4.26}$$

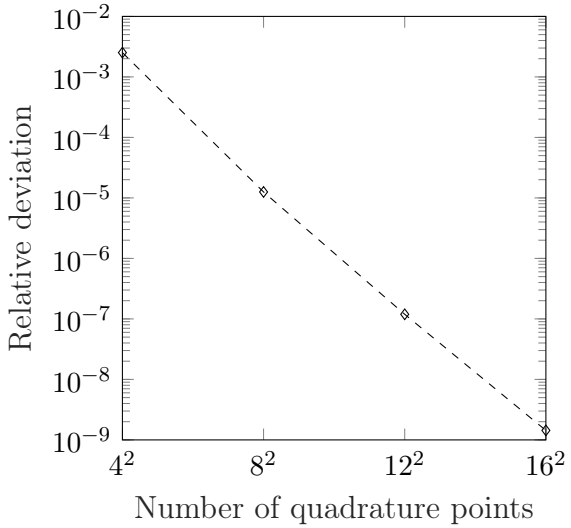

Figure 4.6 – Quadrature convergence for I_4.

Figure 4.6 shows the convergence for the regular 2D integral. We can see that the Gauss-Legendre quadrature is adequate, and 12 points (in each direction) will be used to perform these integrals.

In some cases, we will have to integrate on a cell with a source placed at one of its sides. For instance, when the source is at the boundary and the cell is directly adjacent to it. In this case we define the integral I_5 with a source at $\zeta = -1$, $\eta = 0$ and $r = \sqrt{(\zeta+1)^2 + \eta^2}$.

$$\Psi_{I5} = (1 + 2(\zeta + 0.5) + 2(\eta + 0.5) + 4(\zeta + 0.5)(\eta + 0.5)) \tag{4.27}$$

$$I_5 = \Psi_{I5} \exp\left(\frac{\zeta+1}{2}\right)\left[-\mu \mathrm{K}_1(\mu r)\frac{\zeta+1}{r} - 0.5\mathrm{K}_0(\mu r)\right] \tag{4.28}$$

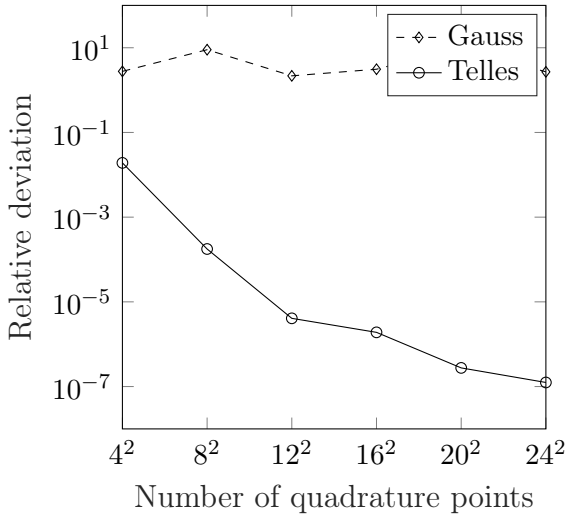

Figure 4.7 – Quadrature convergence for I_5.

Figure 4.7 shows that the Telles transformation is necessary. In this case, we chose to perform these integrals with 24 points in each direction.

Since the cells are discontinuous, we have yet one type of integral to be solved, when the source is placed at an internal node of a cell. We then define the integrals I_{6a} and I_{6b} with a source at $\zeta = -0.5$, $\eta = -0.5$ and $r = \sqrt{(\zeta+0.5)^2 + (\eta+0.5)^2}$.

$$\Psi_{I6a} = (1 - 2(\zeta + 0.5) - 2(\eta + 0.5) + 4(\zeta + 0.5)(\eta + 0.5)) \tag{4.29}$$

$$I_{6a} = \Psi_{I6a} \exp\left(\frac{\zeta + 0.5}{2}\right)\left[-\mu \mathrm{K}_1(\mu r)\frac{\zeta + 0.5}{r} - 0.5\mathrm{K}_0(\mu r)\right] \tag{4.30}$$

$$\Psi_{I6b} = (1 + 2(\zeta + 0.5) - 2(\eta + 0.5) - 4(\zeta + 0.5)(\eta + 0.5)) \tag{4.31}$$

$$I_{6b} = \Psi_{I6b} \exp\left(\frac{\zeta + 0.5}{2}\right)\left[-\mu \mathrm{K}_1(\mu r)\frac{\zeta + 0.5}{r} - 0.5\mathrm{K}_0(\mu r)\right] \tag{4.32}$$

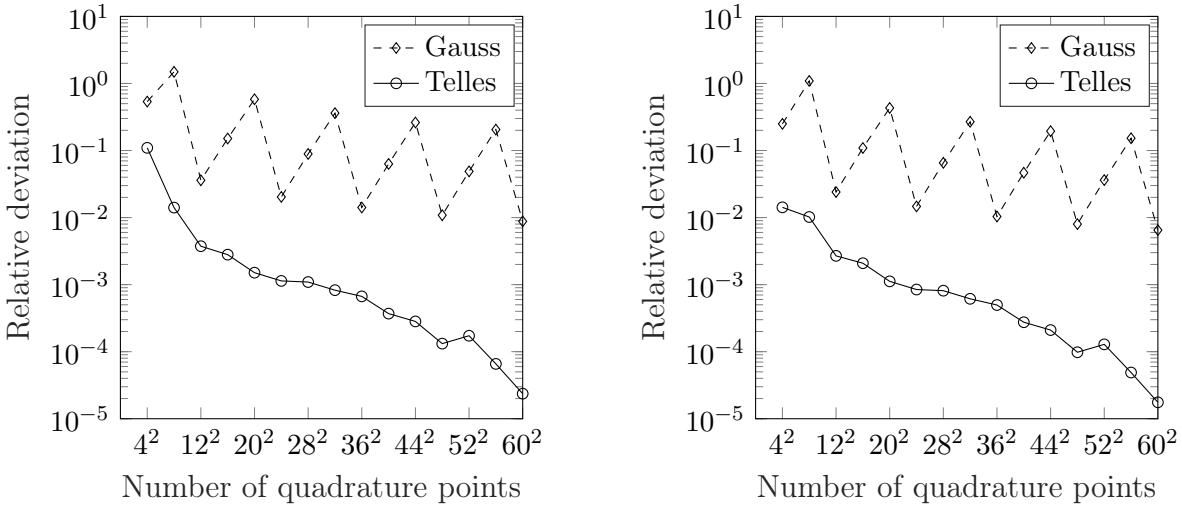

(a) Singular kernel

(b) Regularized by Ψ

Figure 4.8 – Quadrature convergence for (a) I_{6a} and (b) I_{6b}.

Figure 4.8 shows that these integrals are the hardest to perform. Similar to the one-dimensional case, when the source is inside the integration domain, we need more points to evaluate the integral at a similar quality. In these cases, we chose to use 60 points in each direction.

The table below shows the integration technique and the number of integration points utilized in each matrix or vector of Equation 4.14, and for the source position in relation to the integration domain. The number of points was chosen so that the kernels that are regular or have a source at the edge of their integration domain could be performed with a maximum relative deviation of 10^{-6} and the ones with the source at the interior could be performed with a maximum relative deviation of 10^{-4}.

Table 4.1 – Chosen number of quadrature points for each integration scenario.

Matrix/Vector	Source location [1]	Algorithm	Points [2]
$\boldsymbol{H}^b$, $\boldsymbol{G}^b$	Outside	Gauss-Legendre	12
	Edge	Telles	16
	Inside	Telles	40
$\boldsymbol{H}^d$, $\boldsymbol{G}^d$	Outside	Gauss-Legendre	12
$\boldsymbol{B}^b$, $\boldsymbol{b}^b$	Outside	Gauss-Legendre	12
	Edge	Telles	24
$\boldsymbol{B}^d$, $\boldsymbol{b}^d$	Outside	Gauss-Legendre	12
	Inside	Telles	60

[1] May be *outside* of the integration domain, on the *edge* of it, or *inside* it.
[2] Number of points per dimension;

4.4 Chapter Summary

In this chapter, we presented the discrete form of the BDIE in Equation 3.21 and the steps that were taken to form a linear system of matrix equations to be solved. We also analyzed the convergence of the numerical integration schemes used to evaluate the kernels present on the components of the matrices in Equation 4.14.

5 BENCHMARKS

In this chapter, we will compare the results from our numerical model with analytical ones. We will do so in five different cases, chosen in such a way as to showcase the effect of different terms of Equation 3.21. The table below presents the expressions for the coefficients used in each case, as well as the domain Ω where they are defined.

Table 5.1 – Overview of the benchmark cases with the computational domain and the expressions for the coefficients.

Case	Ω	$\boldsymbol{v}$	d	k	S
1	$(0,1)\times(0,1)$	$(Pe,0)$	1	-	-
2	$(1,2)\times(1,2)$	-	x	-	S_0
3	$(1,2)\times(1,2)$	-	$\exp(x+y)$	$(x+y)^{-1}$	$-2\exp(x+y)+1$
4	$(1,2)\times(1,2)$	$(1,1)$	$\frac{x^2+y^2}{x+y}$	-	-
5	$(0,1)\times(0,1)$	$((c_2^2/c_3)(y-c_1)^2,0)$	1	9.724	-

In all five cases the domains were constituted of unitary square regions, represented as cartesian products of the type $(x_i, x_f)\times(y_i, y_f)$. The boundary conditions in each edge of the unity square are of the first kind in $x = x_i$ or $x = x_f$, and of the second kind in $y = y_i$ or $y = y_f$, where x_i, y_i and x_f, y_f are the lower and upper bounds for x and y on the domain.

In every benchmark case, the boundary mesh used will be homogeneous, with element size denoted by h_e. The domain mesh will also be homogeneous, and the cell edge size will be noted by h_c. The boundary element h_e and domain cell h_c sizes are usually not the same, with $h_e < h_c$.

In order to assess the quality of the solution, we will use three Normalized Root Mean Square Deviation (NRMSD) estimators, one for the boundary values of ϕ, one for the boundary values of q_n, and one for the domain values of ϕ. They are defined respectively in Equations 5.1 to 5.3.

$$E_1 = \frac{1}{\bar{\phi}} \sqrt{\frac{1}{n_j} \sum_{j=1}^{n_j} (\phi_j^b - \phi_j^a)^2} \tag{5.1}$$

$$E_2 = \frac{1}{\bar{q_n}} \sqrt{\frac{1}{n_j} \sum_{j=1}^{n_j} (q_{nj}^b - q_{nj}^a)^2} \tag{5.2}$$

$$E_3 = \frac{1}{\bar{\phi}} \sqrt{\frac{1}{n_l} \sum_{l=1}^{n_l} (\phi_l^d - \phi_l^a)^2} \tag{5.3}$$

where ϕ_i^a and q_{ni}^a are the analytical results at node i, while $\bar{\phi}$ and $\bar{q_n}$ are the reference values used for the normalization.

The mesh refinement studies will use the same discretizations throughout the five benchmark cases, since they are all defined in unitary square regions. The first tested element size will be $h_e = 0.2$, and the refinements will be done by halving this value in each step. In cases where there is domain effects, there is the cell-to-element size ratio to be considered. The Figure 5.1a shows the second mesh used for benchmark case 1, a problem without domain effects. Figure 5.1b shows the second mesh used for benchmark cases 2 to 5, containing domain cells and internal physical nodes.

(a) $h_e = 0.1$ (b) $h_e = 0.1$ and $h_c = 0.5$

Figure 5.1 – Second mesh used on the discretization studies. (a) For case 1, boundary mesh only with 40 elements. (b) For cases 2 to 5, mesh with 40 boundary elements and 4 domains cells, for a total of 60 degrees of freedom.

5.1 Case 1 - Advection-diffusion with constant coefficients

The first benchmark to be solved is an advection-diffusion problem with constant coefficients, velocity on the x direction only, and no source. This problem needs only boundary discretization, having no domain effects to be accounted for. The non-null terms of the BDIE are:

$$c_\xi \, \phi_\xi + \int_{\partial\Omega} \phi \, \left(v_n \, \phi^*_\xi + d \, q^*_\xi \right) \, \mathrm{d}l \, - \int_{\partial\Omega} q_n \, d \, \phi^*_\xi \, \mathrm{d}l \, = 0 \tag{5.4}$$

We will impose the following boundary conditions:

$$\phi = 0 \quad \text{in } (0, y) \tag{5.5}$$

$$\phi = 1 \quad \text{in } (1, y) \tag{5.6}$$

$$\frac{\partial \phi}{\partial n} = 0 \quad \text{in } (x, 0) \cup (x, 1) \tag{5.7}$$

where Pe is the Peclet number. This case has an analytical solution, given by:

$$\phi = \begin{cases} x & \text{for Pe} = 0 \\ \frac{exp(\mathrm{Pe}\, x) - 1}{exp(\mathrm{Pe}) - 1} & \text{otherwise} \end{cases} \tag{5.8}$$

Figure 5.2 shows the boundary results of the potential ϕ along x for 5 different Pe numbers. We can see that there is good agreement between the numerical and the analytical solution, even for the higher Péclet numbers. Figure 5.3a shows the evolution of the E_1 NRMSD indicator with mesh refinement, for three Péclet numbers. Notice that for $Pe = 0$, the equation simplifies to a diffusion equation. Figure 5.3b shows the evolution of the three NRMSD indicators for $Pe = 10$ with the mesh refinement. The reference values used for the normalization of the indicators were $\bar{\phi} = 1$ and $\bar{q_n} = (Pe \exp(Pe)/(\exp(Pe) - 1))$.

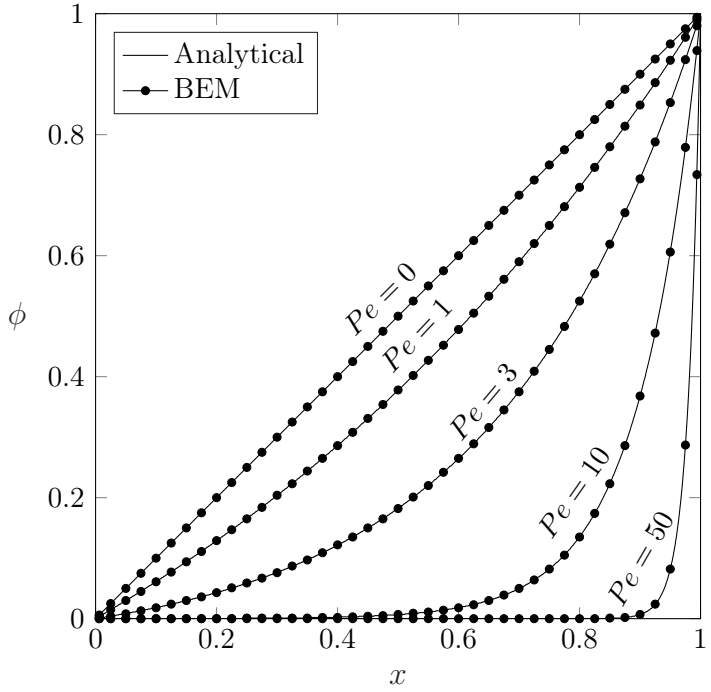

Figure 5.2 – ϕ along x for various Pe numbers. The mesh was formed by 160 boundary elements.

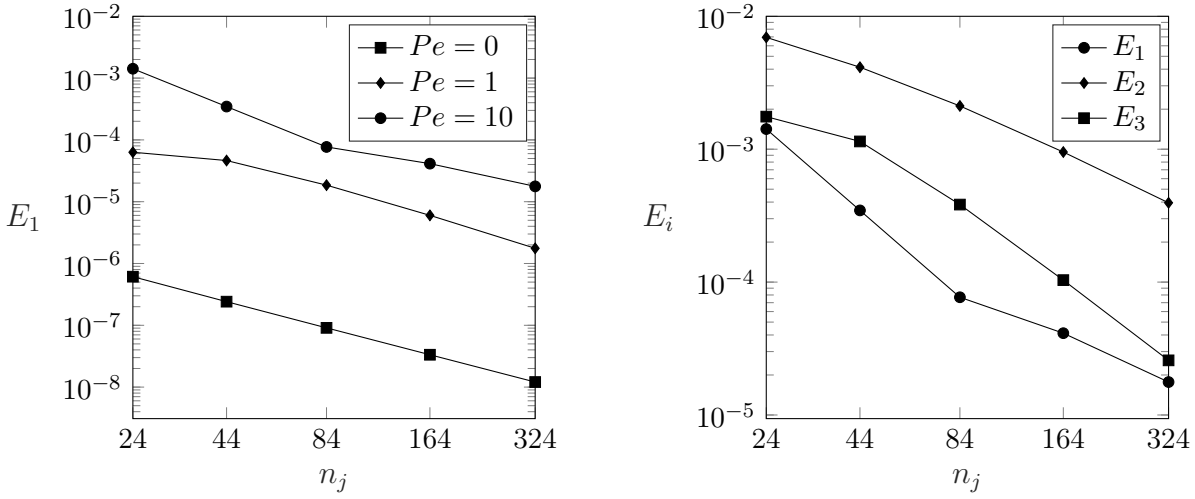

(a) E_1 for $Pe = 0$, 1, and 10.

(b) E_1, E_2, e E_3 for $Pe = 10$.

Figure 5.3 – Variation of the three error estimators for 5 different boundary discretizations, and three different Péclet numbers.

5.2 Case 2 - Diffusion problem with variable diffusivity and constant source

In this benchmark, we will solve the diffusion equation with variable diffusivity and the presence of a constant domain source S_0. We will use the Integral Equation 3.21 to solve the degenerated equation where the velocity field is identically zero. The non-null terms of the BDIE are:

$$c_\xi \, \phi_\xi + \int_{\partial\Omega} \phi \, d \, q^*_\xi \, \mathrm{d}l \; - \int_{\partial\Omega} q_n \, d \, \phi^*_\xi \, \mathrm{d}l \; = \int_\Omega S_0 \phi^*_\xi \mathrm{d}A \; + \int_\Omega \phi \, \nabla d \cdot \nabla \phi^*_\xi \, \mathrm{d}A \tag{5.9}$$

We will impose the following boundary conditions:

$$\phi = 0 \quad \text{in } (1, y) \tag{5.10}$$

$$\phi = 1 \quad \text{in } (2, y) \tag{5.11}$$

$$\frac{\partial \phi}{\partial n} = 0 \quad \text{in } (x, 1) \cup (x, 2) \tag{5.12}$$

This case has an analytical solution, given by:

$$\phi = S_0(1 - x) + \frac{1 + S_0}{\ln 2} \ln x \tag{5.13}$$

Figure 5.4 shows the ϕ boundary results for two values of S_0. The numerical results show good agreement with the analytical ones. Figure 5.5a shows the evolution of the three NRMSD indicators with mesh refinement, for $h_c/h_e = 5$. Figure 5.5b shows the influence of the relative cell to boundary element size on the NRMSD indicator E_1, for a mesh with 160 boundary elements. As can be seen, the relative cell size ranging from 2 (400 cells) to 10 (16 cells) does not seem to have a big influence on the error indicator. The reference values used for the normalization of the indicators were the maximum absolute value of ϕ and q_n.

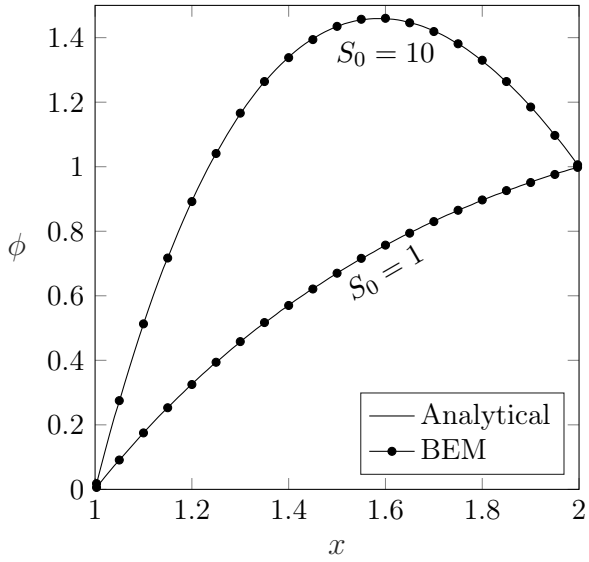

Figure 5.4 – Boundary ϕ along x for two S_0 values, in benchmark 2. The mesh was formed by 80 boundary elements and 25 domain cells.

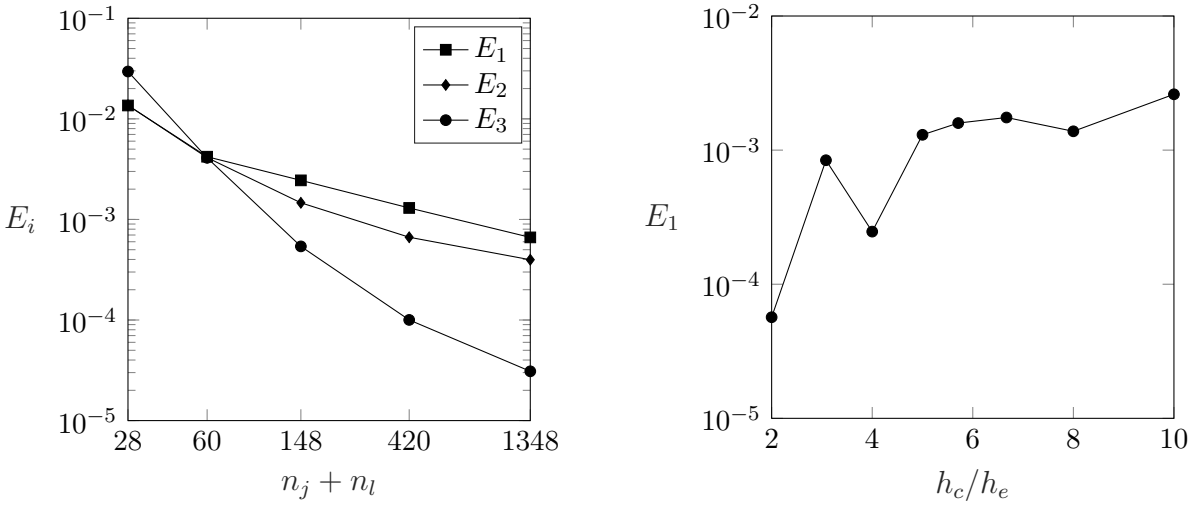

Figure 5.5 – (a) Error estimators for benchmark case 2 with $S_f = 10$ and $h_c/h_e = 5$, considering different discretizations. (b) E_1 for $h_e = 0.025$, varying relative cell size.

5.3 Case 3 - Diffusion-Reaction problem with variable coefficients and variable source

The benchmark case 3 is a problem without a velocity field, and with variable diffusivity, reactivity, and source. This benchmark was built similarly to one of the problems solved by AL-Jawary and Wrobel, 2012. We will again solve a degenerated form of the differential equation (without the advective terms), and the non-null terms of the BDIE are:

$$c_\xi\,\phi_\xi + \int_{\partial\Omega} \phi\, d\, q^*_\xi \,\mathrm{d}l \; - \int_{\partial\Omega} q_n\, d\, \phi^*_\xi \,\mathrm{d}l \; = \int_\Omega S\phi^*_\xi \mathrm{d}A + \\ + \int_\Omega \phi \left[\nabla d \cdot \nabla \phi^*_\xi + \left(\frac{d}{d_\xi} k_\xi - k\right) \phi^*_\xi\right] \mathrm{d}A \quad (5.14)$$

We will impose the following boundary conditions:

$$\phi = 1 + y \quad \text{in } (1, y) \quad (5.15)$$

$$\phi = 2 + y \quad \text{in } (2, y) \quad (5.16)$$

$$\frac{\partial \phi}{\partial n} = -1 \quad \text{in } (x, 1) \quad (5.17)$$

$$\frac{\partial \phi}{\partial n} = 1 \quad \text{in } (x, 2) \quad (5.18)$$

This case has an analytical solution, given by:

$$\phi = x + y \quad (5.19)$$

Figure 5.6 shows surface plots for the variable coefficients and analytical results of ϕ. As it can be seen, especially for d and S_f, the coefficients may have high gradients and complex variations, which have to be interpolated by the cells. Figure 5.7 shows ϕ and q_n boundary values, and the numerical results show good agreement with the analytical ones, except for a small spurious oscillation near the corners for the q_n curves. Figure 5.8a shows the evolution of the three NRMSD indicators with mesh refinement, for $h_c/h_e = 5$. Figure 5.8b shows the influence of the relative cell to boundary element size on the NRMSD indicator E_1, for a mesh with 160 boundary elements. As can be seen, the relative cell size ranging from 2 (400 cells) to 10 (16 cells) does not seem to have a big influence on the error indicator. The reference values used for the normalization of the indicators were $\bar{\phi} = 4$ and $\bar{q_n} = 1$.

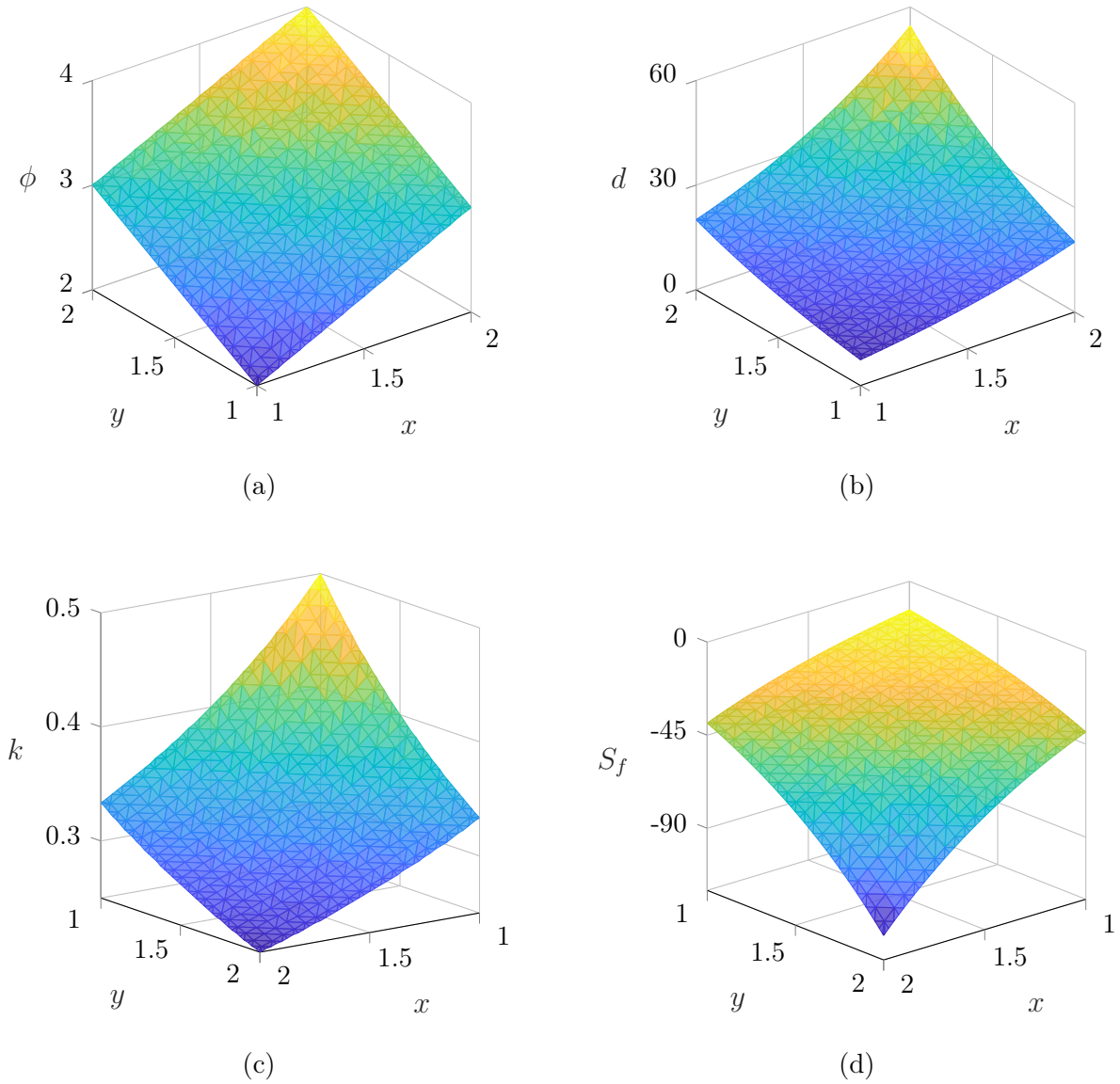

Figure 5.6 – Surface plots for benchmark case 3. (a) ϕ (b) d (c) k (d) S_f.

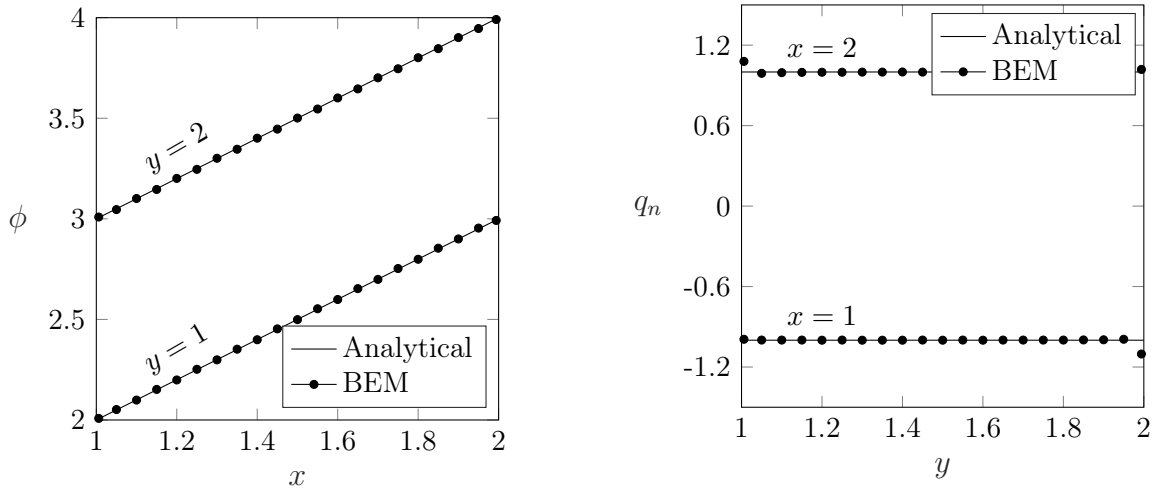

(a) (b)

Figure 5.7 – Boundary results for benchmark case 3. (a) ϕ along x for $y = 1$ and $y = 2$. (b) q_n along y for $x = 1$ and $x = 2$. The mesh was formed by 80 boundary elements and 25 domain cells.

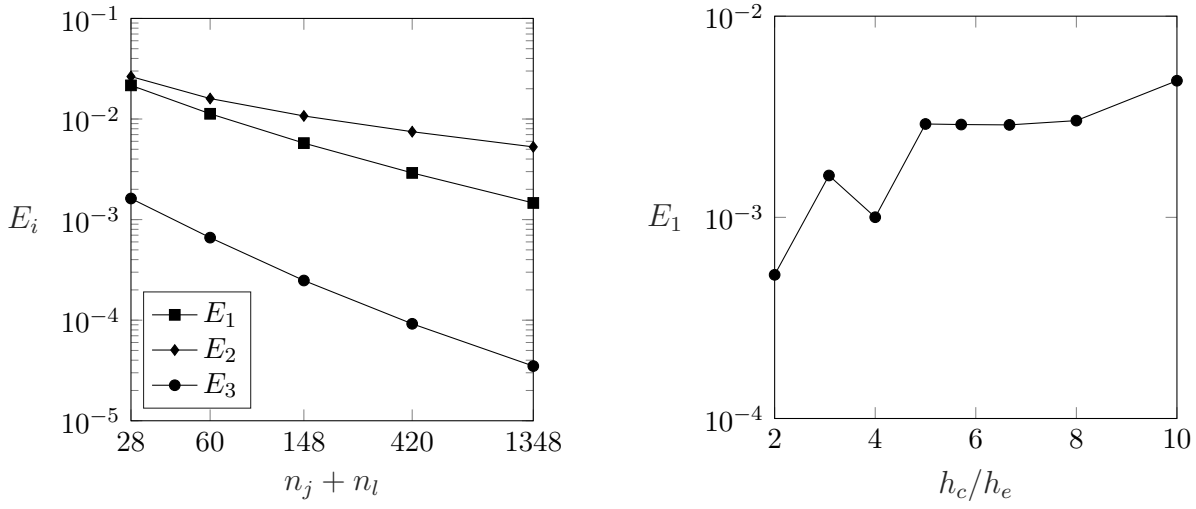

(a) (b)

Figure 5.8 – Error estimators for benchmark case 3. (a) $h_c/h_e = 5$, considering different discretizations. (b) E_1 for $h_e = 0.025$, varying relative cell size.

5.4 Case 4 - Advection-Diffusion problem with variable diffusivity

The fourth benchmark case is a problem with variable diffusivity and a constant velocity field. This problem was also used as a benchmark by Ravnik and Škerget, 2013. The reaction and source terms are identically zero. The non-null terms of the BDIE are:

$$c_\xi\,\phi_\xi + \int_{\partial\Omega} \phi\,\left(v_n\,\phi^*_\xi + d\,q^*_\xi\right)\,\mathrm{d}l\; - \int_{\partial\Omega} q_n\,d\,\phi^*_\xi\,\mathrm{d}l\; = \int_\Omega \phi\,\left[\left(\left(1-\frac{d}{d_\xi}\right)\boldsymbol{v}_\xi + \nabla d\right)\cdot\nabla\phi^*_\xi\right]\mathrm{d}A \quad (5.20)$$

We will impose the following boundary conditions:

$$\phi = (1+y)^2 \quad \text{in } (1,y) \quad (5.21)$$

$$\phi = (2+y)^2 \quad \text{in } (2,y) \quad (5.22)$$

$$\frac{\partial\phi}{\partial n} = -2(x+1) \quad \text{in } (x,1) \quad (5.23)$$

$$\frac{\partial\phi}{\partial n} = 2(x+2) \quad \text{in } (x,2) \quad (5.24)$$

This case has an analytical solution, given by:

$$\phi = (x+y)^2 \quad (5.25)$$

Figure 5.9 shows surface plots for the variable diffusivity and analytical results of ϕ. Figure 5.10 shows ϕ and q_n boundary values, and the numerical results show good agreement with the analytical ones. Figure 5.11a shows the evolution of the three NRMSD indicators with mesh refinement, for $h_c/h_e = 5$. Figure 5.11b shows the influence of the relative cell to boundary element size on the NRMSD indicator E_1, for a mesh with 160 boundary elements. As can be seen, the relative cell size ranging from 2 (400 cells) to 10 (16 cells) does not seem to have a big influence on the error indicator. The reference values used for the normalization of the indicators were $\bar{\phi} = 16$ and $\bar{q_n} = 8$.

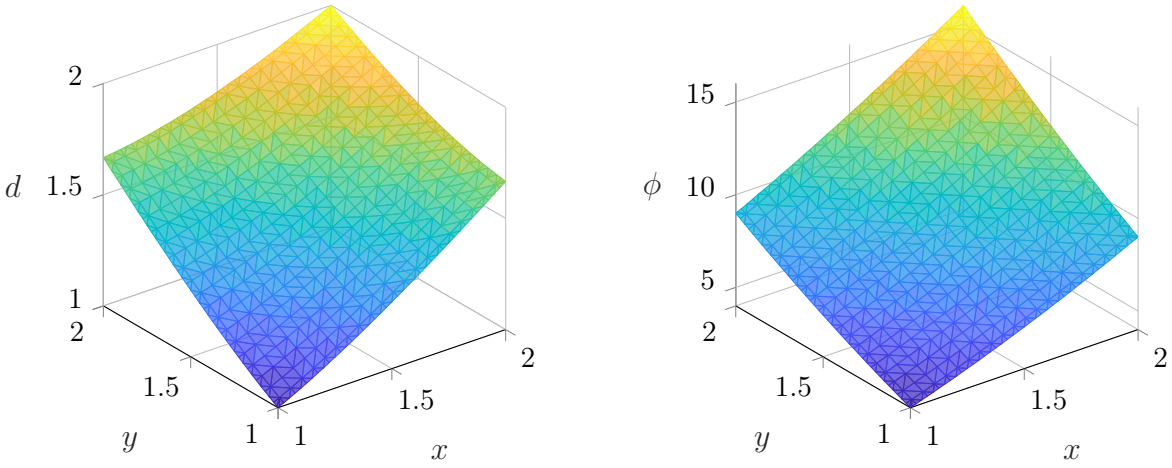

Figure 5.9 – Surface plots for benchmark case 4. (a) d. (b) ϕ.

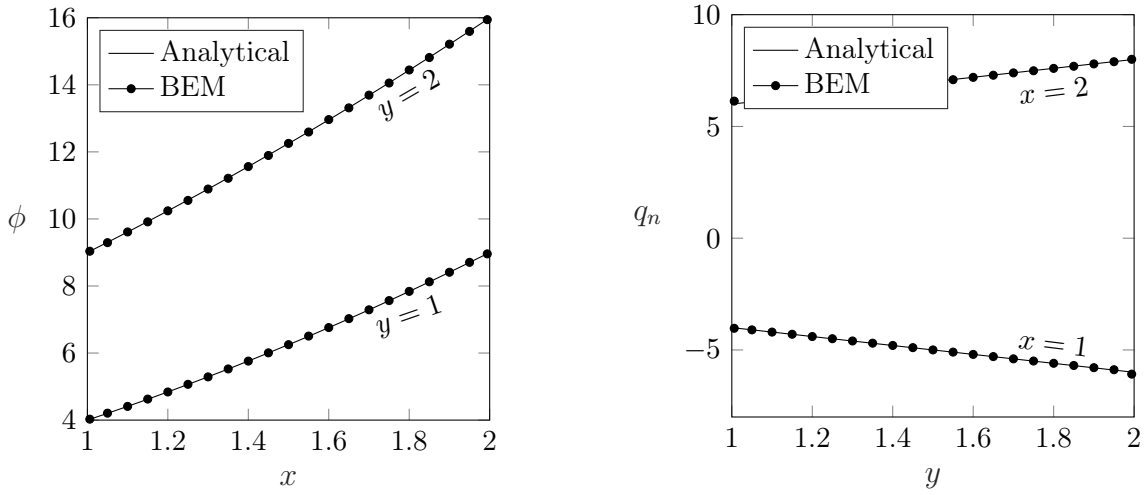

Figure 5.10 – Boundary results for benchmark case 4. (a) ϕ along x for $y = 1$ and $y = 2$. (b) q_n along y for $x = 1$ and $x = 2$. The mesh was formed by 80 boundary elements and 25 domain cells.

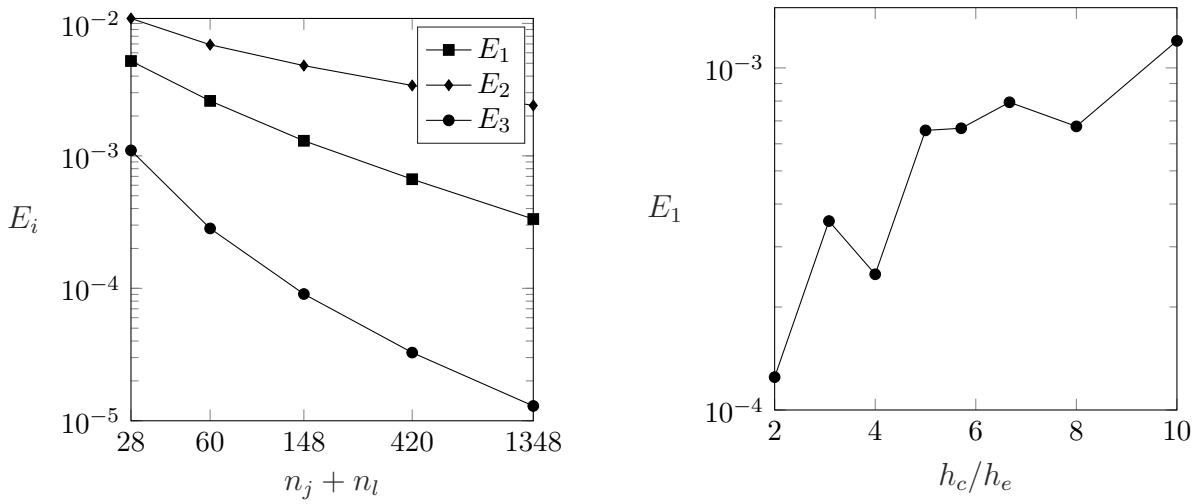

Figure 5.11 – (a) Error estimators for benchmark case 4 with $h_c/h_e = 5$, considering different discretizations. (b) E_1 for $h_e = 0.025$, varying relative cell size.

5.5 Case 5 - Advection-Diffusion-Reaction problem with variable velocity field

This final benchmark case is a problem with variable velocity and constant diffusivity and reaction. This problem was also used as a benchmark by Wrobel and DeFigueiredo, 1991a. The non-null terms of the BDIE are:

$$c_\xi\,\phi_\xi + \int_{\partial\Omega} \phi\,\left(v_n\,\phi^*_\xi + d\,q^*_\xi\right)\,\mathrm{d}l\;-\int_{\partial\Omega} q_n\,d\,\phi^*_\xi\,\mathrm{d}l\;=\int_\Omega \phi\,\left[(\boldsymbol{v}\;-\boldsymbol{v}_\xi)\cdot\nabla\phi^*_\xi\right]\mathrm{d}A \tag{5.26}$$

The expression for the velocity and the imposed boundary conditions are:

$$v_x = \frac{c_2^2}{c_3}\,(y-c_1)^2 \tag{5.27}$$

$$\phi = \bar{\phi}\exp(0.5c_2y^2 - c_1c_2y) \quad \text{in } (0,y) \tag{5.28}$$

$$\phi = \bar{\phi}\exp(0.5c_2y^2 - c_1c_2y + c_3) \quad \text{in } (1,y) \tag{5.29}$$

$$\frac{\partial\phi}{\partial n} = \bar{\phi}c_1c_2\exp(c_3\,x) \quad \text{in } (x,0) \tag{5.30}$$

$$\frac{\partial\phi}{\partial n} = \bar{\phi}c_2(1-c_1)\exp[c_2(0.5-c_1) + c_3\,x] \quad \text{in } (x,1) \tag{5.31}$$

where c_1 is a constant that defines the point in y where the velocity is zero. $c_2 = k - c_3^2$ and $c_3 = \ln\frac{\phi(1,0)}{\phi(0,0)}$ are auxiliary constants. $\bar{\phi}$ is a reference concentration, and will be set

to 300, as in Wrobel and DeFigueiredo, 1991a. This problem has the following analytical solution:

$$\phi = \bar{\phi} \exp\left(\frac{c_2}{2} y^2 - c_1 c_2\, y + c_3\, x\right) \tag{5.32}$$

Figure 5.12a shows v_x as a function of y for two values of c_1. Notice that if $c_1 = 0$, the velocity is zero at one of the boundaries, and the fundamental solution applied there has a different form, with the exponential term being absent as in case 2 of Equation 3.16. The remaining boundaries have the full solution applied, as in case 3 of Equation 3.16.

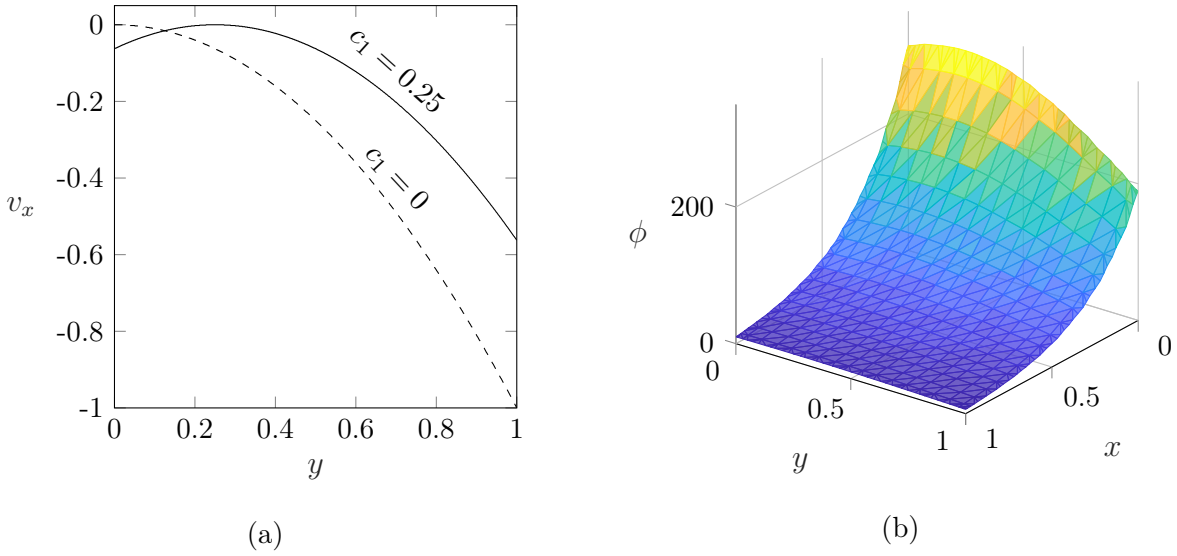

Figure 5.12 – (a) $v_x(y)$ for two values of c_1. (b) Benchmark case 5 ϕ surface plot for $c_1 = 0.25$.

Figure 5.12b shows a ϕ surface plot for benchmark case 5 with $c_1 = 0.25$. Figure 5.13 shows ϕ and q_n boundary values, and the numerical results show good agreement with the analytical ones, with the exception of a small spurious oscillation near the corners for the q_n results. Figure 5.14a shows the evolution of the three NRMSD indicators with mesh refinement, for $h_c/h_e = 5$. Figure 5.14b shows the influence of the relative cell to boundary element size on the NRMSD indicator E_1, for a mesh with 160 boundary elements. As can be seen, the relative cell size ranging from 2 (400 cells) to 10 (16 cells) does not seem to have a big influence on the error indicator. The reference values used for the normalization of the indicators were $\bar{\phi} = 300$ and $\bar{q_n} = 1000$.

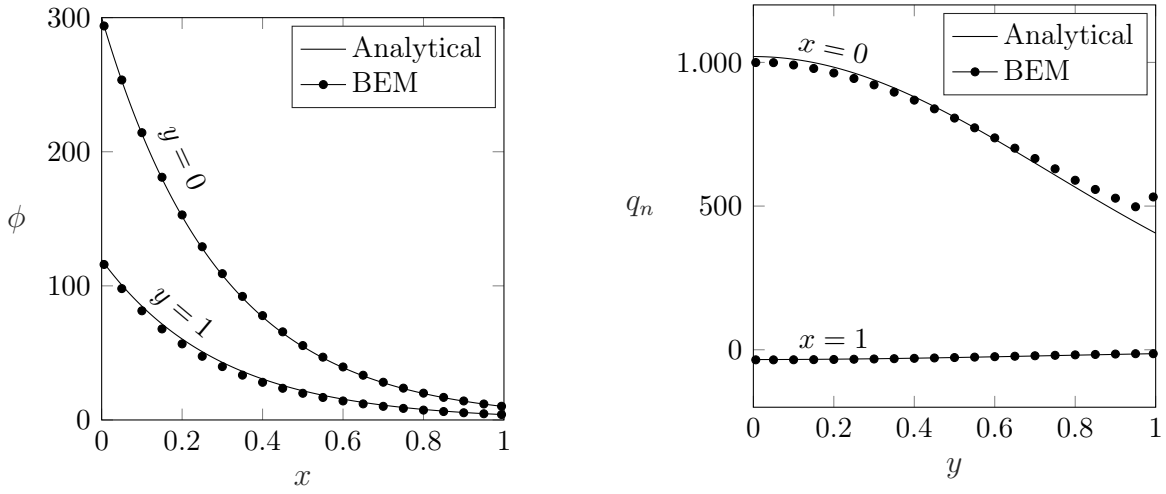

(a) (b)

Figure 5.13 – Boundary results for benchmark case 5 with $c_1 = 0$. (a) ϕ along x for $y = 0$ and $y = 1$. (b) q_n along y for $x = 0$ and $x = 1$. The mesh was formed by 80 boundary elements and 25 domain cells.

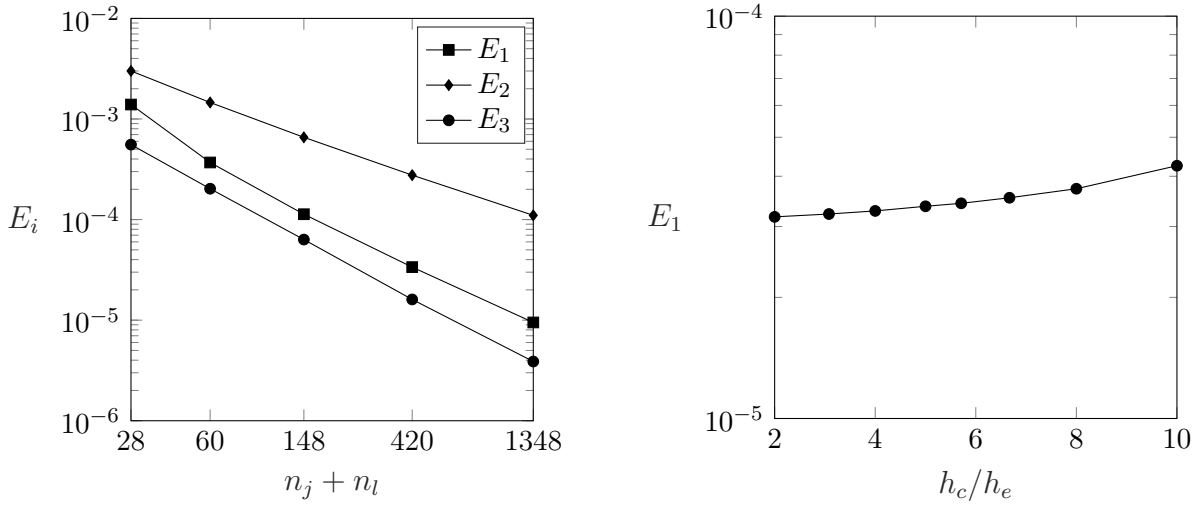

(a) (b)

Figure 5.14 – (a) Error estimators for benchmark case 5 with $h_c/h_e = 5$, considering different discretizations. (b) E_1 for $h_e = 0.025$, varying relative cell size.

5.6 Chapter Summary

In this chapter, we used five different benchmark cases to test the accuracy of the implemented numerical code. It works well for a wide range of Péclet numbers, and considering every coefficient variable in the domain. The same scheme solves both the full equation or degenerated versions of it, such as the diffusion equation. Also, we found that the sensitivity of the solution to the relative cell size utilized is low, meaning that the domain discretization may be coarser than the boundary one.

6 APPLICATIONS

In the previous chapter, we sought to validate the proposed scheme against analytical solutions. In this chapter, we will use the same formulation to solve two practical applications: one in heat transfer and the other in mass transport.

The problems approached here do not have a closed analytical solution. Therefore we will not use the error metrics defined in Equations 5.1 to 5.3. Instead, we will use the mean relative absolute deviation of values in a set of points, between two meshes with different refinements. Let f_i^j be the i-th value chosen for the conversion, referring to the j-th mesh. These values may be either of ϕ or q_n. The relative deviation metric D_j referring to the j-th mesh is then defined as:

$$D_j = \frac{1}{n_f} \sum_{i=1}^{n_f} \left| \frac{f_i^j - f_i^{j-1}}{f_i^j} \right| \tag{6.1}$$

where n_f is the number of values chosen for the mesh refinement study.

6.1 Graetz-Nusselt Problem

This application is the so-called Graetz-Nusselt problem. It consists of a bi-dimensional, fully developed fluid flow between parallel plates at uniform temperature suddenly entering a region whose walls are set at a different temperature. The temperature of the fluid before entering the region is called T_{in}, and the temperature of the new region's walls is called T_{wall}. The figure below shows a schematic representation of the semi-infinite channel with the referred temperatures. Additionally, the properties of the fluid are constant throughout the domain, as well as the pressure gradient and velocity profile. The flow is laminar and in permanent regime.

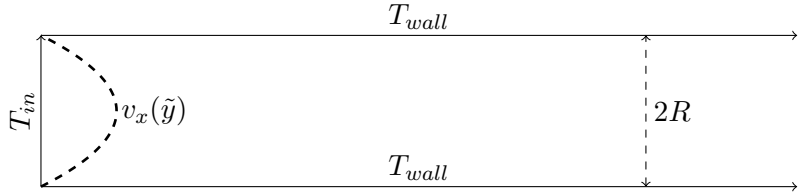

Figure 6.1 – Representation of the Graetz-Nusselt problem's domain and boundary conditions.

We will consider the dimensionless version of the problem. In this case, ϕ will represent the dimensionless excess of temperature, defined in 6.2 Let R be the half-width of the channel, used as a reference length, v_0 be the mean velocity on the channel, d be the thermal diffusivity, and Pe be the Péclet number. Let us consider the origins of the coordinate system to be the middle of the inlet, with the domain being $\Omega = (0, \infty) \times (-R, R)$. Then the dimensionless coordinates $\tilde{x}$, $\tilde{y}$, and dimensionless velocity field λ will be:

$$\phi = \frac{T(x,y) - T_{wall}}{T_{in} - T_{wall}} \tag{6.2}$$

$$\tilde{x} = \frac{x}{R} \tag{6.3}$$

$$\tilde{y} = \frac{y}{R} \tag{6.4}$$

$$Pe = \frac{v_0 R}{d} \tag{6.5}$$

$$\lambda = \frac{3}{2} Pe \left(1 - \tilde{x}^2\right) \tag{6.6}$$

The dimensionless differential problem to be solved will be:

$$\lambda \frac{\partial \phi}{\partial \tilde{x}} - \frac{\partial^2 \phi}{\partial \tilde{x}^2} - \frac{\partial^2 \phi}{\partial \tilde{y}^2} = 0 \tag{6.7}$$

with the following boundary conditions:

$$\phi = 1, \quad \text{for } \tilde{x} = 0 \tag{6.8}$$

$$\phi = 0, \quad \text{for } \tilde{y} = |1| \tag{6.9}$$

$$\phi \to 0, \quad \text{for } \tilde{x} \to \infty \tag{6.10}$$

This problem has been approached extensively in the literature. In order to get an analytical solution, usually the diffusion in the $\tilde{x}$ direction is neglected, and the solution is found using separation of variables, with the results given by an infinite series. One example of such an approximate solution is given by Prins et al., 1951.

Our numerical solution will not disregard the diffusion in the $\tilde{x}$ direction, but it will consider a truncated domain, going from $\tilde{x} = 0$ to $\tilde{x} = 10$. The boundary condition at the end of this domain will be that of null normal diffusive flux, or $q_n = 0$. It is adequate when the Péclet number is high, or the temperature steady-state has been reached.

The first step is to perform a mesh quality analysis. We began with a mesh whose boundary element size was $h_e = 0.2$, and the cells' edge length was 2.5 times the boundary

element size. The mesh was refined by halving the boundary element length and keeping the cell size to element size ratio constant. The first mesh for this problem is represented in Figure 6.2, and the reference values used to calculate the mesh deviation metric D_j were the concentration at the truncated end of the channel, with $\tilde{y} = \{-0.8, -0.6, \cdots, 0.8\}$, and the normal flux at the bottom wall, with $\tilde{x} = \{0.2, 0.4, \cdots, 1.8\}$. The comparison has a total of 18 values, 9 for the temperature at the boundary, and 9 for flux. As seen on the benchmarks, the internal values usually present a smaller error, so we chose to use only boundary values for the mesh study. For the mesh analysis we chose to use the problem with $Pe = 10$. Table 6.1 shows the evolution of the D_j indicator for several refinement iterations.

Table 6.1 – Discretization study for the Graetz-Nusselt problem.
Case with $Pe = 10$, and $h_c/h_e = 2.5$.

Mesh	h_e	D_j
1	0.200	-
2	0.100	$3.0918\ 10^{-2}$
3	0.050	$0.4144\ 10^{-2}$
4	0.025	$0.0564\ 10^{-2}$

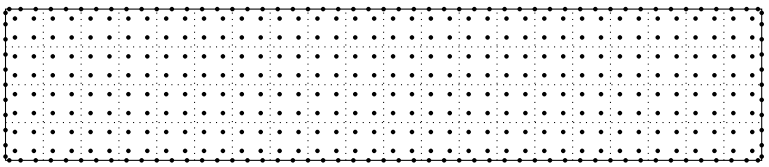

Figure 6.2 – First mesh used for the discretization study. The filled circles are physical nodes, the solid lines are boundary elements and the dotted lines are cell divisions.

As can be seen from the table above, the solution deviation from one mesh to the other is small. We chose to use the mesh 2, with $h_e = 0.1$, to perform the rest of the calculations, since it has a deviation of less than half a percentage point in relation to mesh 3. Is uses 1524 degrees of freedom, being 240 boundary elements and 320 domain cells. Figure 6.3 shows the dimensionless temperature along the central line of the channel ($\tilde{y} = 0$), for four Péclet numbers. The case with $Pe = 0$, corresponds to a pure diffusive problem. The higher the Péclet number is, the greater is the channel length needed

to achieve a uniform temperature. Figure 6.4 shows color maps for the dimensionless temperature considering Péclet values of 1, 5 and 10.

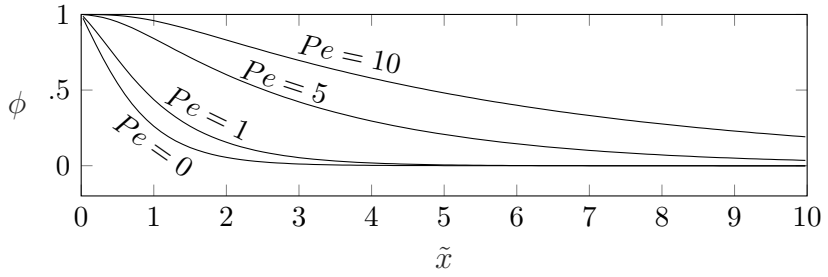

Figure 6.3 – ϕ along $\tilde{x}$ for $\tilde{y} = 0$, considering 4 different Pe numbers.

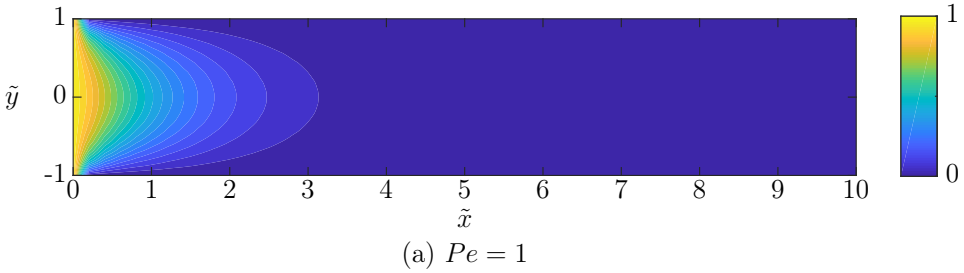

(a) $Pe = 1$

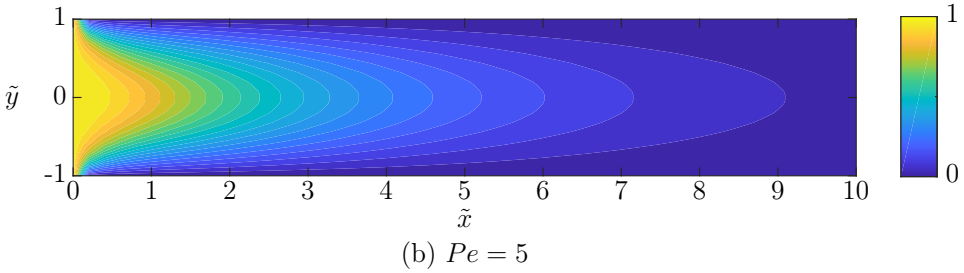

(b) $Pe = 5$

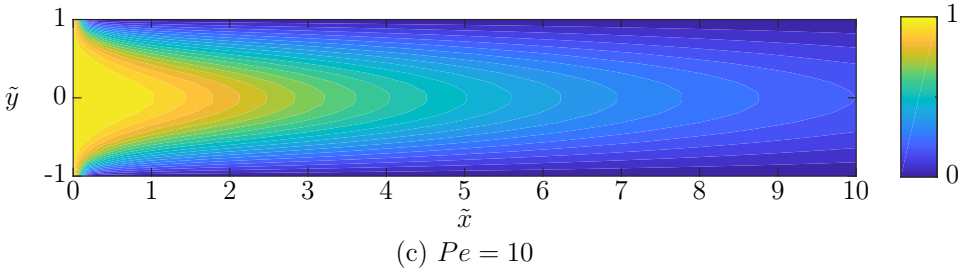

(c) $Pe = 10$

Figure 6.4 – Numerical results for the Graetz-Nusselt problem. All calculated using a mesh with $h_e = 0.1$ e $h_c = 0.25$. (a) $Pe = 1$, (b) $Pe = 5$, (c) $Pe = 10$.

6.2 Pollutant Dispersion on the Atmospheric Boundary Layer

In this section, we will solve a pollutant plume for a point discharge in a typical atmospheric boundary layer flow. This source representation is appropriate for modeling the kind of pollutant discharge that does not significantly change the flow. The considered wind profiles will be classical logarithmic profiles, adequate for flat terrain and a neutrally stratified boundary layer. The expression for these wind profiles is given by:

$$v_x(y) = C \ln\left(\frac{y + y_0}{y_0}\right) \tag{6.11}$$

where C is the friction velocity divided by the Von Kárman constant, and y_0 is the roughness length.

We will consider four cases, the combination of two wind power classes and two terrain types. The wind power classes were defined according to the Wind energy resource atlas of the United States [Elliott et al., 1987] and the terrain roughness values accordingly to the Guide to Meteorological Instruments and Methods of Observation [World Meteorological Organization, 2014]. The values for C and y_0 are shown in the table below, and the wind profiles are represented on Figure 6.5.

Table 6.2 – Wind profile information.

Case number	Power Class	Terrain	$C(m/s)$	$y_0(m)$
I	1	Suburb	0.3767	1.00
II	1	Open field	0.3767	0.03
III	4	Suburb	0.9086	1.00
IV	4	Open field	0.9086	0.03

For all cases, we will consider a uniform turbulent diffusivity of $10\text{m}^2/\text{s}$. In a RANS k-ε model, for example, this diffusivity would vary with height. However, since we are not solving the flow, we considered it to be constant throughout the domain. We also considered no type of linear decay on the pollutant.

The domain, represented in Figure 6.6, consists of a rectangular region 200m high and 400m long. The air flows in the positive x direction and has $\phi = 0$ at the inlet. We considered the diffusive flux to be null at the rest of the boundaries, implying no penetration on the ground, that the upper boundary was higher than the pollutant plume,

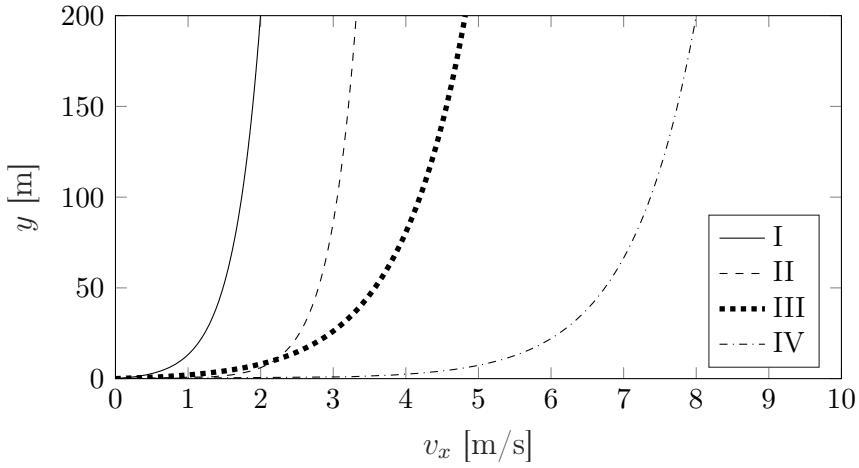

Figure 6.5 – Velocity profiles for each studied case.

and that the flow at the outlet is advective dominant. We considered a unitary point source, located at the point $\boldsymbol{x}_k = (31m, 31m)$.

For the discretization quality study, we used case VI, because it has the highest Péclet number, and thus will be the most difficult to solve numerically. We began with mesh with a boundary element length of 8m, and cell to element size ratio of 10. This mesh is represented in Figure 6.7. In each refinement step, we divided the element length by two, and kept the cell to element size ratio constant. Table 6.3 shows the D_j metric for a sequence of meshes. It was calculated using the boundary concentration at every 20m for $y = 0$ and at every 15m for $x = 400$, for a total of 32 points.

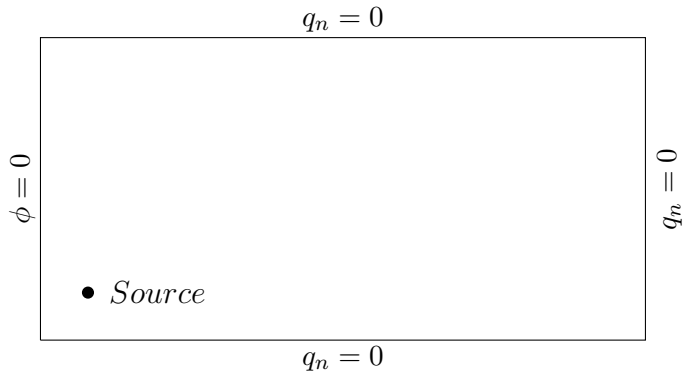

Figure 6.6 – Representation of the pollutant dispersion problem's domain and boundary conditions.

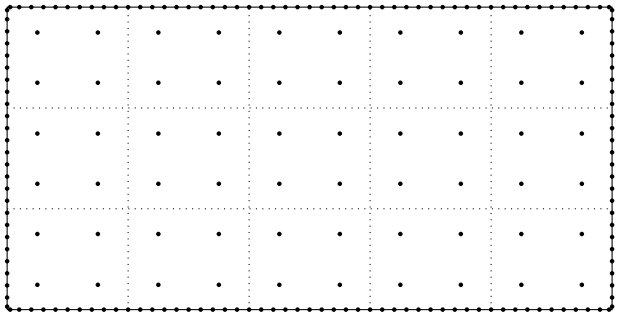

Figure 6.7 – First mesh used for the discretization study. The filled circles are physical nodes, the solid lines are boundary elements and the dotted lines are cell divisions.

Table 6.3 – Discretization study for the pollutant dispersion problem. Study for case IV, with $h_c/h_e = 10$.

Mesh	h_e	D_j
1	8	-
2	4	3.156
3	2	0.228
4	1	0.178
5	.5	0.069

We chose to use mesh 4, whose deviation indicator had a 6.9% difference in relation to mesh 5. The mesh has 4404 degrees of freedom, being 1200 boundary elements and 800 domain cells. This mesh was used for all subsequent results.

Figure 6.8 shows 20 concentration contours for cases I and II, with wind power class 1 and suburban and open field terrains, respectively. Figure 6.9 shows 20 concentration contours for cases III and IV, with wind power class 4 and suburban and open field terrains, respectively. The stronger the wind, the smaller the concentration becomes, as expected.

Figure 6.10 shows concentration profiles at several locations in the domain. In Figure 6.10a, we can see the concentration at $x = 52.5m$, approximately 20m away from the source, plotted against the height. There is a concentration peak near the location of the source. Figure 6.10b shows the concentration at $x = 232.5m$, approximately 200m away from the source, plotted against the height. At this distance, the concentration peak is on the ground, for every case but IV. Figure 6.10c shows the concentration profiles at $y = 2.5m$, plotted against the distance to the source. As can be seen, for stronger winds,

there is not a noticeable concentration amount near the location of the source, while for case I (weaker wind) there is.

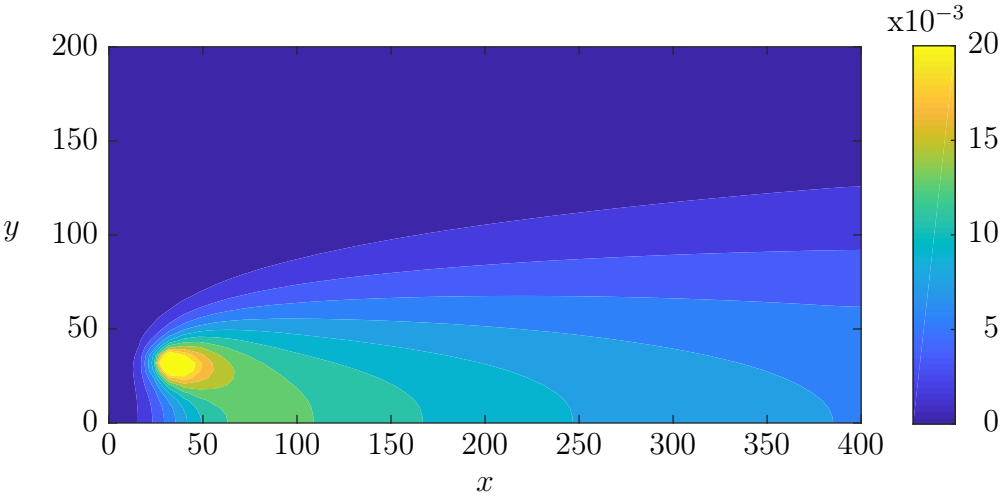

(a) Case I: wind power class I and suburban roughness.

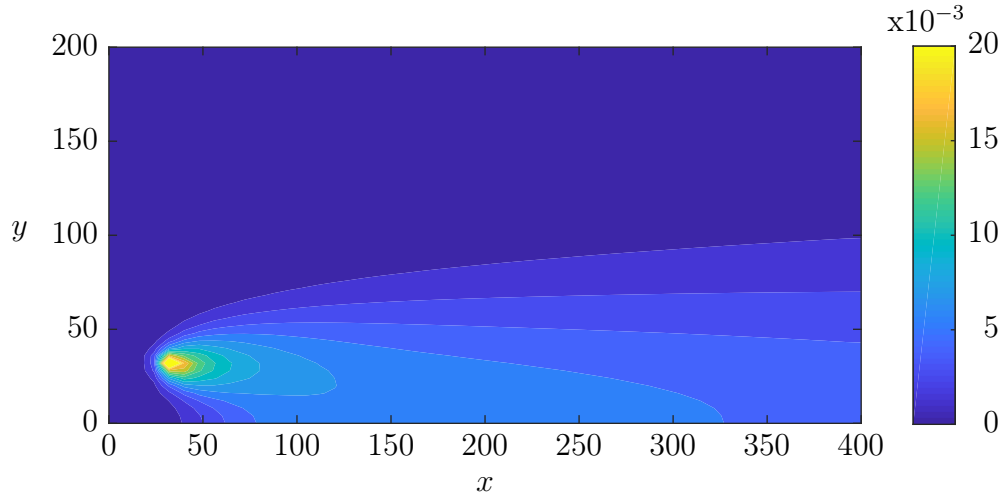

(b) Case II: wind power class I and open field roughness.

Figure 6.8 – Concentration color-map for Cases I and II.

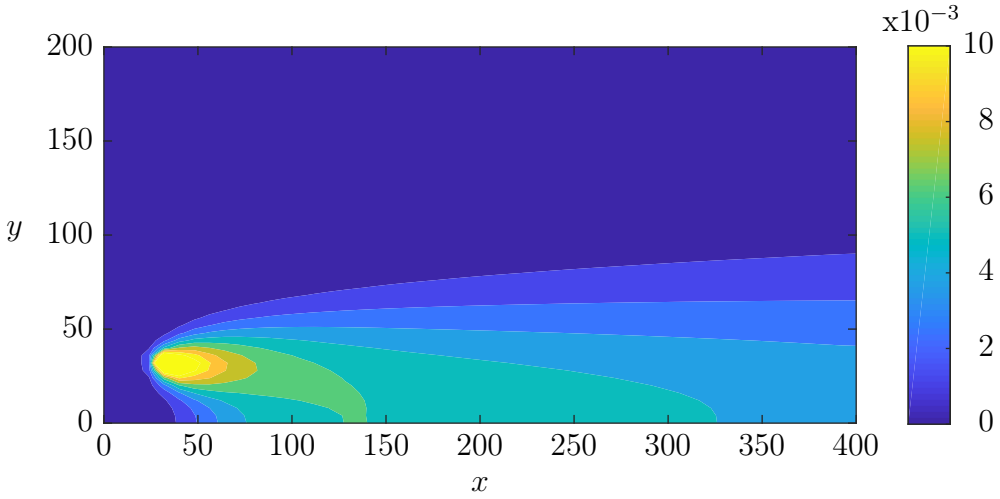

(a) Case III: wind power class IV and suburban roughness.

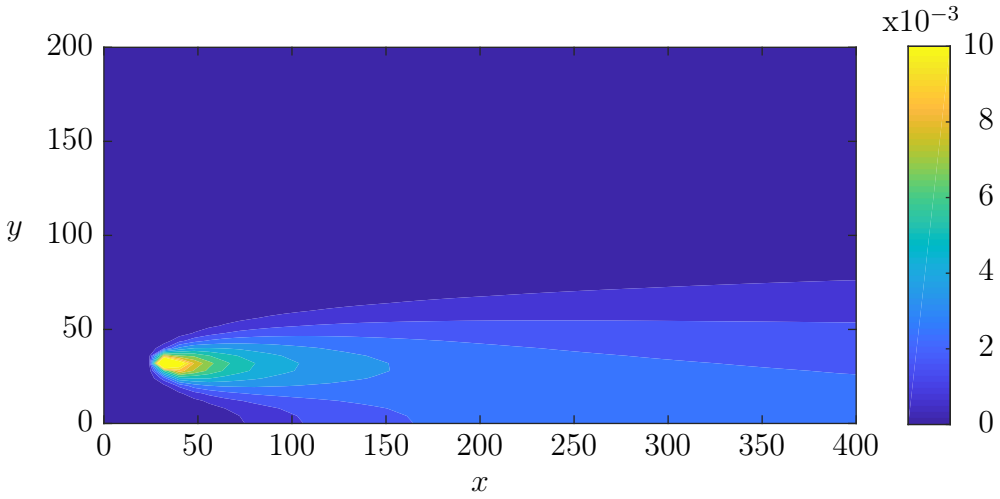

(b) Case IV: wind power class IV and open field roughness.

Figure 6.9 – Concentration color-map for Cases III and IV.

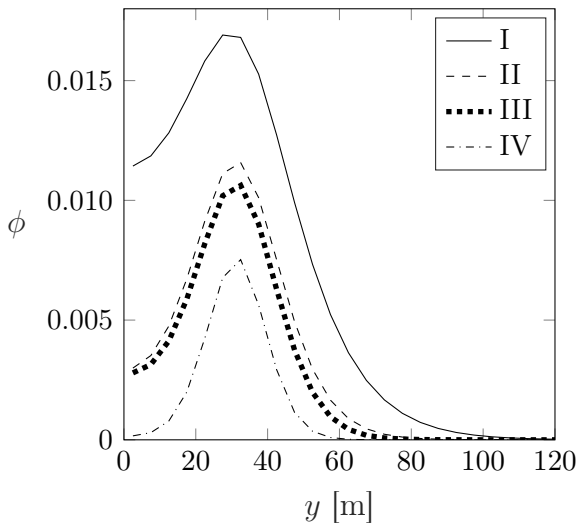

(a) ϕ along $x = 52.5m$.

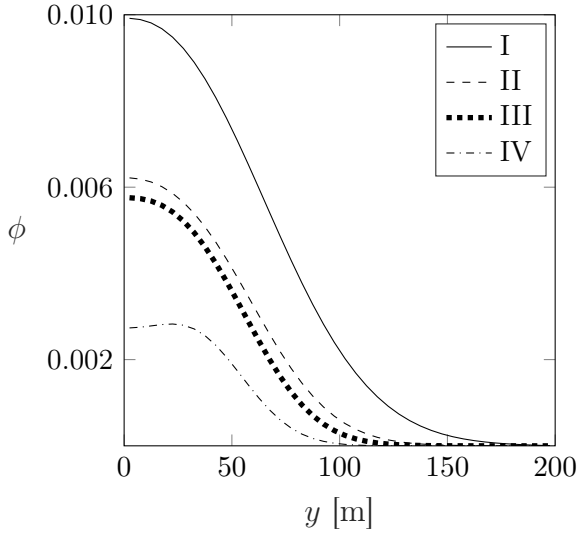

(b) ϕ along $x = 232.5m$.

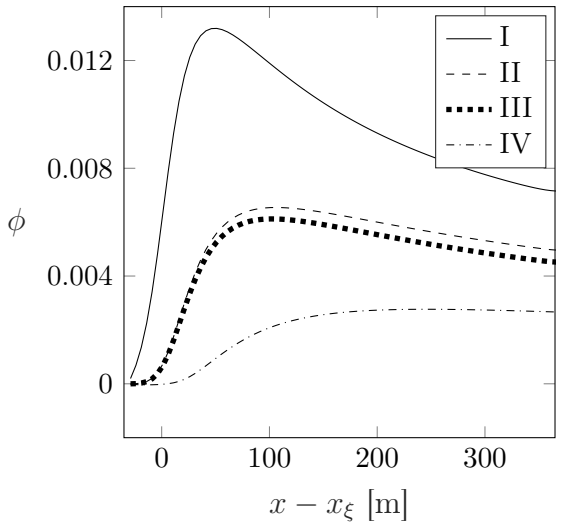

(c) ϕ along $y = 2.5m$.

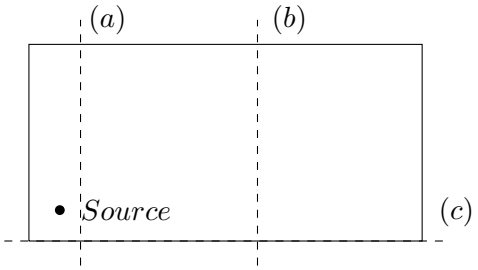

Figure 6.10 – Concentration profiles for (a) $x = 52.5m$ (b) $x = 232.5m$ and (c) $y = 2.5m$.

7 CONCLUSIONS

In this work, an integral equation formulation was derived do deal with linear passive scalar transport problems that may have coefficients and source term that vary throughout their domain. The implemented scheme was validated with benchmark cases and used to solve two applications. Among the contributions and conclusions of this work are:

- The integral formulation developed is a type of gradient-free BDIE, and builds upon the ones present in the literature by considering a linear reaction term in addition to the advective and diffusive terms.

- We proposed a version of the fundamental solution that uses a scaled Bessel function instead of the traditional one. This version avoids numerical overflow of the exponential terms and underflow of the Bessel terms, thus it is stable for large Péclet numbers and large domains where the traditional fundamental solution may present numerical instabilities.

- The BDIE was discretized and solved via the boundary element method. Our scheme uses as the weighting function the fundamental solution with coefficients coinciding with the source point. This reduces to the maximum the contribution of the domain in relation to the boundary. However, our scheme differs when it allows for the fundamental solution to degenerate by having a null velocity vector. By doing this, the same integral equation and the same numerical implementation can be used to solve diffusion or diffusion-reaction problems.

- By implementing a scheme to solve the advection-diffusion-reaction equation with variable coefficients, we made the resulting numerical code versatile. For instance, our scheme could solve scalar transport in an arbitrary incompressible flow configuration computed via Navier-Stokes.

- The proposed numerical scheme was tested against analytical solutions in five different benchmark cases. The cases were chosen in such a way that every term on the integral equation would be dominant in at least one problem. The scheme proved to be efficient in solving these benchmark problems, having the normalized

root-mean square deviation indicators below 1% for meshes with 1348 degrees of freedom. Also, the proposed methodology was used to study two applications: heat transfer for laminar flow in a duct and pollutant transport for a point source in typical atmospheric boundary layer wind profiles.

7.1 Suggestions for further work

This work has many possible ways to be expanded. Among them:

- Expand this formulation to the tri-dimensional and/or transient case.
- Consider fundamental solution in semi-planes in order to consider semi-infinite domains.
- Couple the scalar transport with a Navier-Stokes solver. It is worth noticing that the formulation presented here can incorporate an arbitrary field of turbulent viscosity.
- Use a radial integration method to rewrite the domain integrals as boundary ones. This method, when coupled with radial basis interpolation functions, is meshless on the domain and capable of representing steeper gradients using a smaller number of points if compared that of cell interpolation.
- Use a technique to go from a $\mathcal{O}(N^2)$ complexity to a $\mathcal{O}(N \log N)$ or $\mathcal{O}(N)$ complexity. That would allow us to tackle problems with a larger number of degrees of freedom in a reasonable computational time. This reduction in complexity can be achieved by applying the sub-domain technique or methods such as the fast multipole.

REFERENCES

AL-Bayati, S. A. and Wrobel, L. C. The dual reciprocity boundary element formulation for convection-diffusion-reaction problems with variable velocity field using different radial basis functions, **International Journal of Mechanical Sciences**, vol. 145, p. 367–377, 2018a.

AL-Bayati, S. A. and Wrobel, L. C. A novel dual reciprocity boundary element formulation for two-dimensional transient convection–diffusion–reaction problems with variable velocity, **Engineering Analysis with Boundary Elements**, vol. 94, p. 60–68, 2018b.

AL-Bayati, S. A. and Wrobel, L. C. Radial integration boundary element method for two-dimensional non-homogeneous convection–diffusion–reaction problems with variable source term, **Engineering Analysis with Boundary Elements**, vol. 101, p. 89–101, 2019.

AL-Jawary, M. and Wrobel, L. Numerical solution of the two-dimensional Helmholtz equation with variable coefficients by the radial integration boundary integral and integro-differential equation methods, **International Journal of Computer Mathematics**, vol. 89, 2012.

Aral, M. M. and Tang, Y. A boundary-only procedure for transient transport problems with or without first-order chemical reaction, **Applied Mathematical Modelling**, vol. 13(3), p. 130–137, 1989.

Azis, M. I. Standard-BEM solutions to two types of anisotropic-diffusion convection reaction equations with variable coefficients, **Engineering Analysis with Boundary Elements**, vol. 105, p. 87–93, 2019.

Azis, M. I., Kasbawati, Haddade, A., and Thamrin, S. A. On some examples of pollutant transport problems solved numerically using the boundary element method, **Journal of Physics: Conference Series**, vol. 979, p. 012075, 2018.

Blobner, J., Hriberšek, M., and Kuhn, G. Dual reciprocity BEM–BDIM technique for conjugate heat transfer computations, **Computer Methods in Applied Mechanics and Engineering**, vol. 190(8), p. 1105–1116, 2000.

Bokota, A. and Iskierka, S. An analysis of the diffusion-convection problem by the boundary element method, **Engineering Analysis with Boundary Elements**, vol. 15(3), p. 267–275, 1995.

Bozkaya, C. and Tezer-Sezgin, M. **DRBEM Solution of the Double Diffusive Convective Flow**. In *Numerical Mathematics and Advanced Applications ENUMATH 2015*, Lecture Notes in Computational Science and Engineering, pages 13–21. Springer International Publishing, 2016.

Brebbia, C. and Dominguez, J. Boundary element methods for potential problems, **Applied Mathematical Modelling**, vol. 1, 1977.

Brebbia, C. and Dominguez, J. **Boundary Elements, An Introductory Course**. WIT Pree, Southampton, UK, 1992.

Brebbia, C. A. **Introduction to boundary element methods**. In Brebbia, C. A., editor, *Recent advances in boundary element methods, Proceedings of first international confeerence on boundary element methods*. Pentech: University of Southampton, 1978.

Brebbia, C. A. The birth of the boundary element method from conception to application, **Engineering Analysis with Boundary Elements**, vol. 77, p. iii – x, 2017.

Brebbia, C. A. and Skerget, P. Diffusion-convection problems using boundary elements, **Advances in Water Resources**, vol. 7(2), p. 50–57, 1984.

Bui, T. T. and Popov, V. Domain decomposition boundary element method with overlapping sub-domains, **Engineering Analysis with Boundary Elements**, vol. 33(4), p. 456–466, 2009a.

Bui, T. T. and Popov, V. **The radial basis integral equation method for convection-diffusion problems**. pages 95–104, New Forest, UK, 2009b.

Carrer, J. A. M., Cunha, C. L. N., and Mansur, W. J. The boundary element method applied to the solution of two-dimensional diffusion–advection problems for non-isotropic materials, **Journal of the Brazilian Society of Mechanical Sciences and Engineering**, vol. 39, 2017.

Chan, C. L. and Chandra, A. An algorithm for handling corners in the boundary element method: Application to conduction-convection equations, **Applied Mathematical Modelling**, vol. 15(5), p. 244–255, 1991.

Chandra, A. and Chan, C. L. A Boundary Element Method Formulation for Design Sensitivities in Steady-State Conduction-Convection Problems, **Journal of Applied Mechanics**, vol. 59(1), p. 182–190, 1992.

Chanthawara, K. and Kaennakham, S. A Local-Adaptive Multiquadric Shape Parameter Applied with DRBEM to Convection-Diffusion Problem, **Journal of Telecommunication, Electronic and Computer Engineering (JTEC)**, vol. 10(1-9), p. 141–146–146, 2018.

Chanthawara, K., Kaennakham, S., and Toutip, W. The numerical study and comparison of radial basis functions in applications of the dual reciprocity boundary element method to convection-diffusion problems, **AIP Conference Proceedings**, vol. 1705(1), p. 020029, 2016.

Cheng, A. H.-D. and Cheng, D. T. Heritage and early history of the boundary element method, **Engineering Analysis with Boundary Elements**, vol. 29(3), p. 268–302, 2005.

Cholewa, R., Nowak, A. J., and Wrobel, L. C. Application of BEM and sensitivity analysis to the solution of the governing diffusion–convection equation for a continuous casting process, **Engineering Analysis with Boundary Elements**, vol. 28(4), p. 389–403, 2004.

Cunha, C. L. N., Carrer, J. A. M., Oliveira, M. F., and Costa, V. L. A study concerning the solution of advection–diffusion problems by the Boundary Element Method, **Engineering Analysis with Boundary Elements**, vol. 65, p. 79–94, 2016.

Dargush, G. F. and Grigoriev, M. M. **Efficient Boundary Element Methods for the Time-Dependent Convective Diffusion Equation**. pages 875–886. American Society of Mechanical Engineers Digital Collection, 2008.

DeSilva, S. J., Lik Chan, C., Chandra, A., and Lim, J. Boundary element method analysis for the transient conduction – convection in 2-D with spatially variable convective velocity, **Applied Mathematical Modelling**, vol. 22(1), p. 81–112, 1998.

Driessen, B. J. and Dohner, J. L. A finite element–boundary element method for advection–diffusion problems with variable advective fields and infinite domains, **International Journal of Heat and Mass Transfer**, vol. 44(11), p. 2183–2191, 2001.

Ehrenpreis, L. Solution of Some Problems of Division: Part II. Division by a Punctual Distribution, **American Journal of Mathematics**, vol. 77(2), p. 286–292, 1955.

Elliott, D., Holladay, C., Barchet, W., Foote, H., and Sandusky, W. Wind energy resource atlas of the United States, 1987.

Enokizono, M. and Nagata, S. Convection-diffusion analysis at high Peclet number by the boundary element method, **IEEE Transactions on Magnetics**, vol. 28(2), p. 1651–1654, 1992.

Florez, W. F., Power, H., and Chejne, F. Numerical solution of thermal convection problems using the multidomain boundary element method, **Numerical Methods for Partial Differential Equations**, vol. 18(4), p. 469–489, 2002.

Fredholm, J. Solution d'un probleme fondamental de la Theorie de l'elasticite, **Arkiv for Matematk, Astronomi och Fysk 2**, vol. 28, p. 3–8, 1906.

Friedman, M. and Shaw, R. Diffraction of pulse by cylindrical obstacles of arbitrary cross section, **Journal of Applied Mechanics**, vol. 29, 1962.

Gao, X.-W. The radial integration method for evaluation of domain integrals with boundary-only discretization, **Engineering Analysis with Boundary Elements**, vol. 26, 2002.

Gao, X.-W., Peng, H.-F., and Liu, J. A boundary-domain integral equation method for solving convective heat transfer problems, **International Journal of Heat and Mass Transfer**, vol. 63, p. 183–190, 2013.

Grigoriev, M. M. and Dargush, G. F. Boundary element methods for transient convective diffusion. Part I: General formulation and 1D implementation, **Computer Methods in Applied Mechanics and Engineering**, vol. 192(39), p. 4281–4298, 2003a.

Grigoriev, M. M. and Dargush, G. F. Boundary element methods for transient convective diffusion. Part II: 2D implementation, **Computer Methods in Applied Mechanics and Engineering**, vol. 192(39), p. 4299–4312, 2003b.

Grigoriev, M. M. and Dargush, G. F. Boundary element methods for transient convective diffusion. Part III: Numerical examples, **Computer Methods in Applied Mechanics and Engineering**, vol. 192(39), p. 4313–4335, 2003c.

Grigoriev, M. M. and Dargush, G. F. Accuracy and efficiency of higher-order boundary element methods for steady convective heat diffusion in three-dimensions, **Engineering Analysis with Boundary Elements**, vol. 28(12), p. 1475–1491, 2004a.

Grigoriev, M. M. and Dargush, G. F. Efficiency and Accuracy of Higher-Order Boundary-Element Methods for Steady Convective Heat Diffusion, **Numerical Heat Transfer, Part B: Fundamentals**, vol. 45(2), p. 109–133, 2004b.

Grigoriev, M. M. and Dargush, G. F. Accurate Boundary Element Solutions for Highly Convective Unsteady Heat Flows, **Journal of Heat Transfer**, vol. 127(10), p. 1138–1150, 2005a.

Grigoriev, M. M. and Dargush, G. F. A boundary element method for steady convective heat diffusion in three-dimensions, **Computer Methods in Applied Mechanics and Engineering**, vol. 194(18), p. 2109–2125, 2005b.

Grigoriev, M. M. and Dargush, G. F. Efficiency of boundary element methods for time-dependent convective heat diffusion at high Peclet numbers, **Communications in Numerical Methods in Engineering**, vol. 21(4), p. 149–161, 2005c.

Grigor'ev, M. M. A boundary element method for the solution of convective diffusion and burgers' equations, **International Journal of Numerical Methods for Heat & Fluid Flow**, 1994.

Gupta, A., Chan, C. L., and Chandra, A. Bem Formulation for Steady-State Conduction-Convection Problems with Variable Velocities, **Numerical Heat Transfer, Part B: Fundamentals**, vol. 25(4), p. 415–432, 1994.

Hriberšek, M. and Kuhn, G. Conjugate heat transfer by boundary-domain integral method, **Engineering Analysis with Boundary Elements**, vol. 24(4), p. 297–305, 2000.

Ikeuchi, M. and Onishi, K. Boundary element solutions to steady convective diffusion equations, **Applied Mathematical Modelling**, vol. 7(2), p. 115–118, 1983.

Lachat, J. and Watson, J. Effective numerical treatment of boundary integral equations: a formulation for three-dimensional elastostatics., **International Journal on Numerical Methods in Engineering**, vol. 10, 1976.

Lauricella, G. Sull' integrazione delle equazioni dei corpi elastici isotropi, **Rendiconto Accademia dei Lincei**, vol. 15, p. 426–432, 1907.

Li, B. Q. A Newton-Based Boundary Element Method for Nonlinear Convective Diffusion Problems, **Numerical Heat Transfer, Part B: Fundamentals**, vol. 23(3), p. 369–385, 1993.

Li, B. Q. and Evans, J. W. Boundary element solution of heat convection-diffusion problems, **Journal of Computational Physics**, vol. 93(2), p. 255–272, 1991.

Lim, J., Chan, C. L., and Chandra, A. A bem analysis for transient conduction—convection problems, **International Journal of Numerical Methods for Heat & Fluid Flow**, 1994.

Malgrange, B. Existence et approximation des solutions des équations aux dérivées partielles et des équations de convolution, **Annales de l'Institut Fourier**, vol. 6, p. 271–355, 1956.

Maplesoft, a division of Waterloo Maple Inc. **Maple release 15**. Waterloo, Ontario, 2011.

Massonnet, C. E. and Morelle, P. **The Origin of the Boundary Element Method and its Variants (Opening address)**. In Brebbia, C. A., Wendland, W. L., and Kuhn, G., editors, *Mathematical and Computational Aspects*, pages 1–10, Berlin, Heidelberg. Springer Berlin Heidelberg, 1987.

MATLAB. **9.4.0.813654 (R2018a)**. The MathWorks Inc., Natick, Massachusetts, 2018.

Nardini, B. and Brebbia, C. A new approach to free vibration analysis using boundary elements, **Applied Mathematical Modelling**, vol. 7, 1983.

Partridge, P. W. Dual reciprocity BEM: local versus global approximation functions for diffusion, convection and other problems, **Engineering Analysis with Boundary Elements**, vol. 14(4), p. 349–356, 1994.

Peng, H.-F., Yang, K., Cui, M., and Gao, X.-W. Radial integration boundary element method for solving two-dimensional unsteady convection–diffusion problem, **Engineering Analysis with Boundary Elements**, vol. 102, p. 39–50, 2019.

Ponter, A. and Jawson, M. An integral equation solution of the torsion problem, **Proceedings of the Royal Society**, vol. 273, 1963.

Popov, V. and Power, H. The DRM-MD integral equation method: an efficient approach for the numerical solution of domain dominant problems, **International Journal for Numerical Methods in Engineering**, vol. 44(3), p. 327–353, 1999.

Portapila, M. and Power, H. Iterative schemes for the solution of system of equations arising from the DRM in multi domain approach, and a comparative analysis of the performance of two different radial basis functions used in the interpolation, **Engineering Analysis with Boundary Elements**, vol. 29(2), p. 107–125, 2005.

Prins, J., Mulder, J., and Schenk, J. Heat transfer in laminary flow between parallel plates, **Applied Scientific Research**, vol. 2, 1951.

Qiu, Z. H., Wrobel, L. C., and Power, H. Numerical solution of convection–diffusion problems at high Péclet number using boundary elements, **International Journal for Numerical Methods in Engineering**, vol. 41(5), p. 899–914, 1998.

Rahaim, C. P., Kassab, A. J., and Cavalleri, R. J. Coupled Dual Reciprocity Boundary Element/Finite Volume Method for Transient Conjugate Heat Transfer, **Journal of Thermophysics and Heat Transfer**, vol. 14, 2000.

Ramachandran, P. **Boundary Element Methods in Transport Phenomena**. Computational Mechanics, 1998.

Ramirez Camacho, R. G. and Barbosa, J. R. The boundary element method applied to forced convection heat problems, **International Communications in Heat and Mass Transfer**, vol. 35(1), p. 1–11, 2008.

Rap, A., Elliott, L., Ingham, D. B., Lesnic, D., and Wen, X. DRBEM for Cauchy convection-diffusion problems with variable coefficients, **Engineering Analysis with Boundary Elements**, vol. 28(11), p. 1321–1333, 2004.

Rap, A., Elliott, L., Ingham, D. B., Lesnic, D., and Wen, X. The inverse source problem for the variable coefficients convection-diffusion equation, **Inverse Problems in Science and Engineering**, vol. 15, 2006.

Ravnik, J., Skerget, L., Tibaut, J., and Yeigh, B. Solution of Energy Transport Equation with Variable Material Properties by BEM, **International Journal of Computational Methods and Experimental Measurements**, vol. 5(3), p. 337–347, 2017.

Ravnik, J. and Škerget, L. A gradient free integral equation for diffusion–convection equation with variable coefficient and velocity, **Engineering Analysis with Boundary Elements**, vol. 37(4), p. 683–690, 2013.

Ravnik, J. and Škerget, L. Integral equation formulation of an unsteady diffusion–convection equation with variable coefficient and velocity, **Computers & Mathematics with Applications**, vol. 66(12), p. 2477–2488, 2014.

Rizzo, F. An integral equation approach to boundary value problems of classical elastostatics, **Quarterly of Applied Mathematics**, vol. 25, 1967.

Samec, N. and Škerget, L. Integral formulation of a diffusive–convective transport equation for reacting flows, **Engineering Analysis with Boundary Elements**, vol. 28(9), p. 1055–1060, 2004.

Sedaghatjoo, Z. and Adibi, H. Calculation of domain integrals of two dimensional boundary element method, **Engineering Analysis with Boundary Elements**, vol. 36(12), p. 1917–1922, 2012.

Sharma, A. **Introduction to Computational Fluid Dynamics: Development, Application and Analysis**. Wiley, 2017.

Singh, K. M. and Tanaka, M. Analytical integration of weakly singular integrals in boundary element analysis of Helmholtz and advection–diffusion equations, **Computer Methods in Applied Mechanics and Engineering**, vol. 189(2), p. 625–640, 2000.

Singh, K. M. and Tanaka, M. Dual reciprocity boundary element analysis of transient advection-diffusion, **International Journal of Numerical Methods for Heat & Fluid Flow**, 2003.

Tanaka, Y., Honma, T., and Kaji, I. On mixed boundary element solutions of convection-diffusion problems in three dimensions, **Applied Mathematical Modelling**, vol. 10(3), p. 170–175, 1986.

Tanaka, Y., Honma, T., and Kaji, I. Mixed boundary element solution for three-dimensional convection-diffusion problem with a velocity profile, **Applied Mathematical Modelling**, vol. 11(6), p. 402–410, 1987.

Telles, J. C. F. A self-adaptive co-ordinate transformation for efficient numerical evaluation of general boundary element integrals, **International Journal for Numerical Methods in Engineering**, vol. 24(5), p. 959–973, 1987.

Thanh Tu, B. and Popov, V. **Boundary element dual reciprocity method with overlapping sub-domains**. In *Boundary Elements and Other Mesh Reduction Methods XXX*, volume I, pages 179–187, Maribor, Slovenia. WIT Press, 2008.

World Meteorological Organization. **Guide to Meteorological Instruments and Methods of Observation**. WMO, 2014.

Wrobel, L. C. and DeFigueiredo, D. B. A dual reciprocity boundary element formulation for convection-diffusion problems with variable velocity fields, **Engineering Analysis with Boundary Elements**, vol. 8(6), p. 312–319, 1991a.

Wrobel, L. C. and DeFigueiredo, D. B. Numerical analysis of convection-diffusion problems using the boundary element method, **International Journal of Numerical Methods for Heat & Fluid Flow**, 1991b.

Xu, J. and Zebib, A. An Improved Boundary-Element Method and Its Application to Time-Dependent Convection, **Numerical Heat Transfer, Part B: Fundamentals**, vol. 30(1), p. 93–109, 1996.

Young, G. L., McDonald, K. A., Palazoglu, A., and Ford, W. Boundary Element Solutions for Free Boundary Convection-Diffusion Problems, **Numerical Heat Transfer, Part A: Applications**, vol. 21(3), p. 299–311, 1992.

Zakerdoost, H., Ghassemi, H., and Iranmanesh, M. Solution of Boundary Value Problems Using Dual Reciprocity Boundary Element Method, **Advances in Applied Mathematics and Mechanics**, vol. 9(3), p. 680–697, 2017.

Zhu, S. and Zhang, Y. Improvement on dual reciprocity boundary element method for equations with convective terms, **Communications in Numerical Methods in Engineering**, vol. 10(5), p. 361–371, 1994.

APPENDIX A – Shape Functions

This appendix will present the shape functions used to interpolate the geometry and variables. Section A.1 contains information about the boundary elements' shape functions, and Section A.2 contains information about the domain cells' shape functions.

A.1 One-dimensional interpolation

The shape functions $\psi_j(\zeta)$, corresponding to the node n_j, are defined on the normalized domain in such a way that:

$$\sum_{j=1}^{2} \psi_j = 1 \quad \text{for } \forall \zeta \in [-1, 1]$$

$$\psi_i(n_j) = \delta_{ij}$$

If the element is continuous:

$$\psi_1 = \frac{1}{2}(1 - \zeta) \tag{A.1}$$

$$\psi_2 = \frac{1}{2}(1 + \zeta) \tag{A.2}$$

If the element is discontinuous at the first node:

$$\psi_1 = \frac{1}{2 - \alpha}(1 - \zeta) \tag{A.3}$$

$$\psi_2 = \frac{1}{2 - \alpha}(1 - \alpha + \zeta) \tag{A.4}$$

If the element is discontinuous at the second node:

$$\psi_1 = \frac{1}{2 - \alpha}(1 - \alpha - \zeta) \tag{A.5}$$

$$\psi_2 = \frac{1}{2 - \alpha}(1 + \zeta) \tag{A.6}$$

Since the geometrical interpolation is linear, the Jacobian of the transformation of a boundary element of a certain length l_e to the normalized domain is constant and equal to $l_e/2$. The following figure shows the behavior of each of those shape functions, with $\alpha = 0.5$.

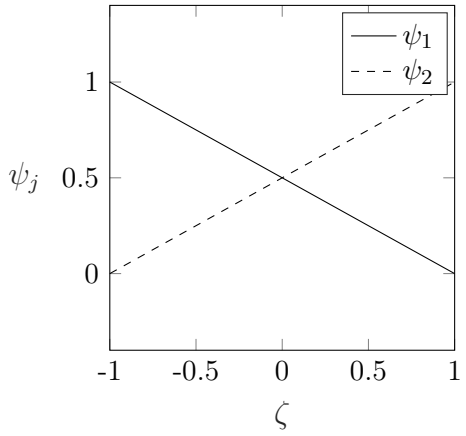

(a) Continuous

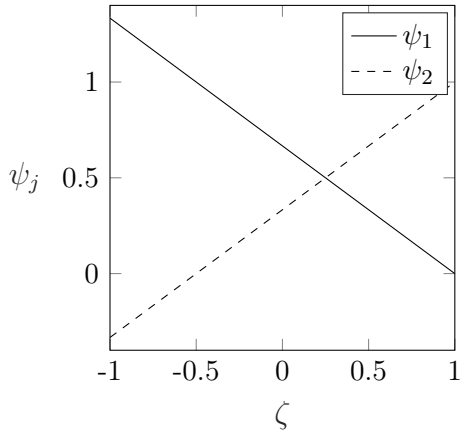

(b) Discontinuous at node 1

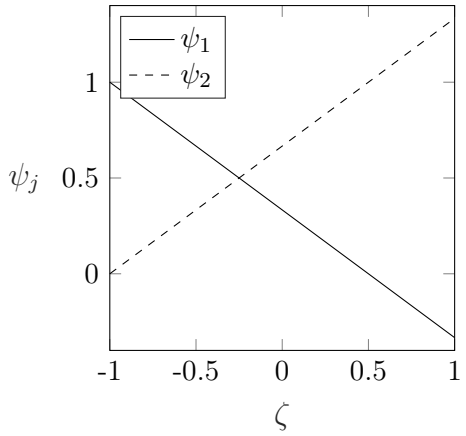

(c) Discontinuous at node 2

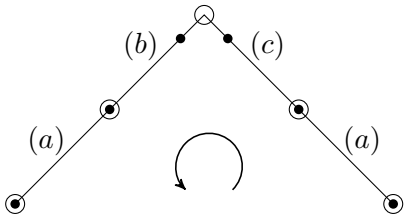

Figure A.1 – Shape functions for the boundary elements. On the bottom right we have a schematic representation of the elements leading to a corner, with the direction of the node numbering. The hollow circles are geometrical nodes, the filled circles are the physical nodes, and the line segments are the elements.

A.2 Two-dimensional interpolation

The shape functions $\Psi_l(\zeta, \eta)$, corresponding to the node n_l, are defined on the normalized domain in such a way that:

$$\sum_{l=1}^{4} \Psi_l = 1 \quad \text{for } \forall(\zeta, \eta) \in [-1, 1] \times [-1, 1]$$

$$\Psi_i(n_l) = \delta_{il}$$

The numbering of the nodes begins at the bottom left node on the normalized domain, and follows on the counter-clockwise sense. There is only the case for discontinuous cells, and the shape functions are:

$$\Psi_1 = \frac{1}{4}\left[1 - \frac{\zeta}{1-\alpha} - \frac{\eta}{1-\alpha} + \frac{\zeta\,\eta}{(1-\alpha)^2}\right] \tag{A.7}$$

$$\Psi_2 = \frac{1}{4}\left[1 + \frac{\zeta}{1-\alpha} - \frac{\eta}{1-\alpha} - \frac{\zeta\,\eta}{(1-\alpha)^2}\right] \tag{A.8}$$

$$\Psi_3 = \frac{1}{4}\left[1 + \frac{\zeta}{1-\alpha} + \frac{\eta}{1-\alpha} + \frac{\zeta\,\eta}{(1-\alpha)^2}\right] \tag{A.9}$$

$$\Psi_4 = \frac{1}{4}\left[1 - \frac{\zeta}{1-\alpha} + \frac{\eta}{1-\alpha} - \frac{\zeta\,\eta}{(1-\alpha)^2}\right] \tag{A.10}$$

these functions are shown in Figure A.2.

The Jacobian of the transformation of a cell with geometrical nodes (x_l, y_l) to the one on the normalized domain is given by:

$$J = \left|\frac{\partial x}{\partial \zeta}\frac{\partial y}{\partial \eta} - \frac{\partial x}{\partial \eta}\frac{\partial y}{\partial \zeta}\right| \tag{A.11}$$

$$\frac{\partial x}{\partial \zeta} = \frac{1}{4}\left[x_1(\eta-1) - x_2(\eta-1) + x_3(\eta+1) - x_4(\eta+1)\right] \tag{A.12}$$

$$\frac{\partial x}{\partial \eta} = \frac{1}{4}\left[x_1(\zeta-1) - x_2(\zeta+1) + x_3(\zeta+1) - x_4(\zeta-1)\right] \tag{A.13}$$

$$\frac{\partial y}{\partial \zeta} = \frac{1}{4}\left[y_1(\eta-1) - y_2(\eta-1) + y_3(\eta+1) - y_4(\eta+1)\right] \tag{A.14}$$

$$\frac{\partial y}{\partial \eta} = \frac{1}{4}\left[y_1(\zeta-1) - y_2(\zeta+1) + y_3(\zeta+1) - y_4(\zeta-1)\right] \tag{A.15}$$

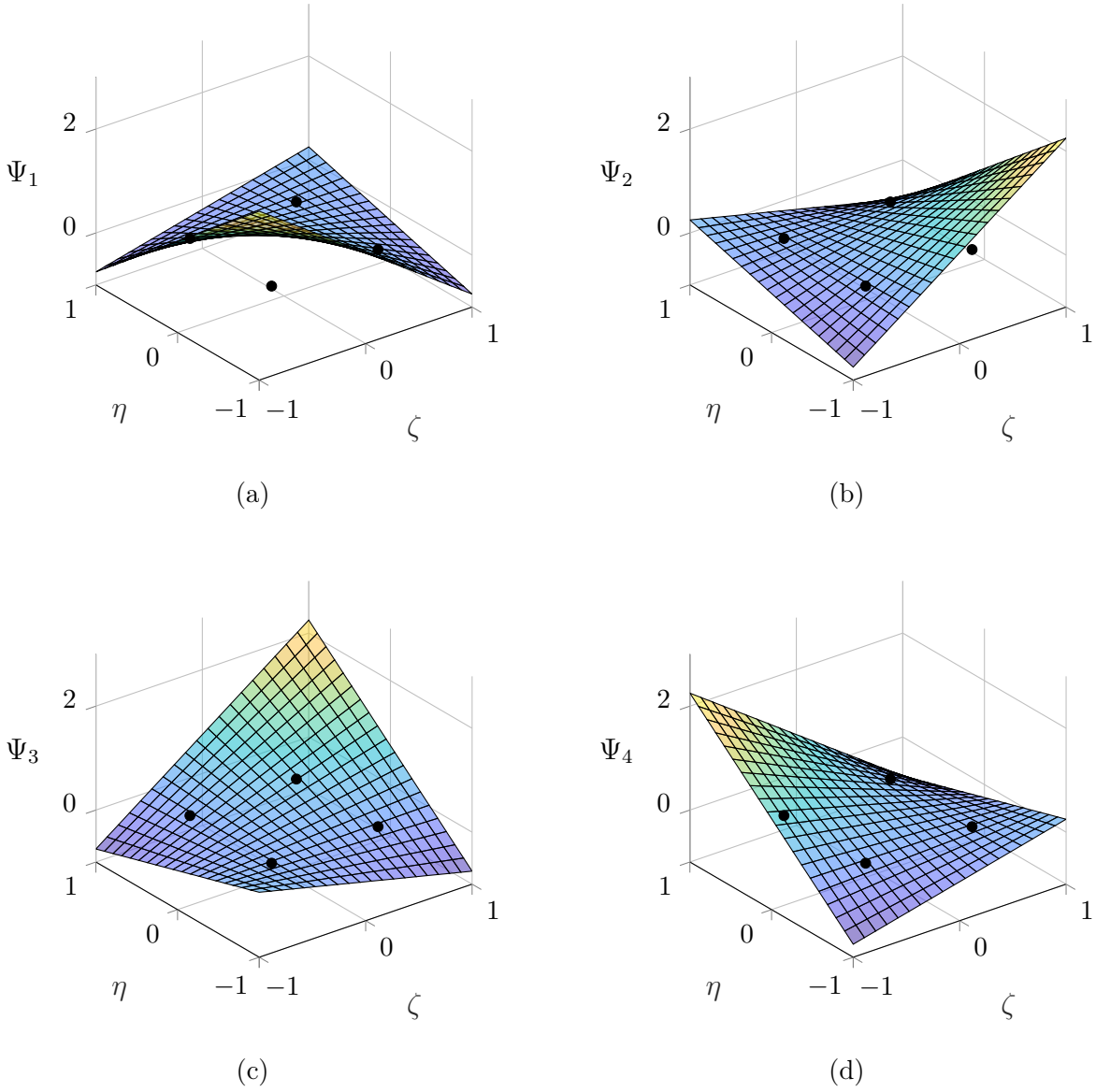

Figure A.2 – Shape functions for a discontinuous domain cell with $\alpha = 0.5$. (a) Ψ_1, (b) Ψ_2, (c) Ψ_3, (d) Ψ_4

APPENDIX B – Telles cubic coordinate transformation

The transformation presented in this chapter is the cubic coordinate transformation proposed by [Telles, 1987] to deal with weakly singular integrals. Let $r_t \in [0, 1]$ be an aggressiveness factor. The proposed transformation must be a mapping of the space onto itself, $\varphi(-1) = -1$, and $\varphi(1) = 1$. The Jacobian of it must be equal to r_t at a given point ζ_t - if the kernel has a singularity, r_t must be zero if we want to concentrate the points near a high gradient region, then r_t mat vary. The closest to zero it is, the more concentrated the quadrature points become. Additionally, it is required that the Jacobian of the transformation has a local extreme at $\zeta = \zeta_t$. The transformation is defined by:

$$\varphi(\zeta) = t_3\zeta^3 + t_2\zeta^2 + t_1\zeta + t_0 \tag{B.1}$$

$$J = 3t_3\zeta^2 + 2t_2\zeta + t_1 \tag{B.2}$$

$$t_3 = \frac{1 - r_t}{p_1} \tag{B.3}$$

$$t_2 = \frac{-3(1 - r_t)p_2}{p_1} \tag{B.4}$$

$$t_3 = \frac{r_t + 3p_2^2}{p_1} \tag{B.5}$$

$$t_4 = \frac{3(1 - r_t)p_2}{p_1} \tag{B.6}$$

$$p_1 = 1 + 3p_2^2 \tag{B.7}$$

$$p_2 = \sqrt[3]{-p_3 + \sqrt{p_3^2 + p_4^3}} + \sqrt[3]{-p_3 - \sqrt{p_3^2 + p_4^3}} + \frac{\zeta_t}{1 + 2r_t} \tag{B.8}$$

$$p_3 = \frac{1}{2(1 + 2r_t)}\left[\left(\zeta_t(3 - 2r_t) - \frac{2\zeta_t^3}{1 + 2r_t}\right)\frac{1}{1 + 2r_t} - \zeta_t\right] \tag{B.9}$$

$$p_4 = \frac{1}{3(1 + 2r_t)^2}\left[4r_t(1 - r_t) + 3(1 - \zeta_t^2)\right] \tag{B.10}$$

Notice that if $r_t = 1$ the above transformation degenerates to the identity, with $J = 1$. Furthermore, if $\zeta_t \to \pm\infty$, the transformation also degenerates into the identity.